Impaired uptake of conjugated bile acids and hepatitis b virus pres1-binding in na(+) -taurocholate cotransporting polypeptide knockout mice

Slijepcevic, Davor ; Kaufman, Christina ; Wichers, Catharina G K ; Gilglioni, Eduardo H ; Lempp, Florian A ; Duijst, Suzanne ; de Waart, Dirk R ; Oude Elferink, Ronald P J ; Mier, Walter ; Stieger, Bruno ; Beuers, Ulrich ; Urban, Stephan ; van de Graaf, Stan F J

Abstract: UNLABELLED: The Na(+) -taurocholate cotransporting polypeptide (NTCP) mediates uptake of conjugated bile acids (BAs) and is localized at the basolateral membrane of hepatocytes. It has recently been recognized as the receptor mediating hepatocyte-specific entry of hepatitis B virus and hepatitis delta virus. Myrcludex B, a peptide inhibitor of hepatitis B virus entry, is assumed to specifically target NTCP. Here, we investigated BA transport and Myrcludex B binding in the first Slc10a1-knockout mouse model (Slc10a1 encodes NTCP). Primary Slc10a1(-/-) hepatocytes showed absence of sodium-dependent taurocholic acid uptake, whereas sodium-independent taurocholic acid uptake was unchanged. In vivo, this was manifested as a decreased serum BA clearance in all knockout mice. In a subset of mice, NTCP deficiency resulted in markedly elevated total serum BA concentrations, mainly composed of conjugated BAs. The hypercholanemic phenotype was rapidly triggered by a diet supplemented with ursodeoxycholic acid. Biliary BA output remained intact, while fecal BA excretion was reduced in hypercholanemic Slc10a1(-/-) mice, explained by increased Asbt and Ost / expression. These mice further showed reduced Asbt expression in the kidney and increased renal BA excretion. Hepatic uptake of conjugated BAs was potentially affected by down-regulation of OATP1A1 and up-regulation of OATP1A4. Furthermore, sodium-dependent taurocholic acid uptake was inhibited by Myrcludex B in wild-type hepatocytes, while Slc10a1(-/-) hepatocytes were insensitive to Myrcludex B. Finally, positron emission tomography showed a complete abrogation of hepatic binding of labeled Myrcludex B in Slc10a1(-/-) mice. CONCLUSION: The Slc10a1-knockout mouse model supports the central role of NTCP in hepatic uptake of conjugated BAs and hepatitis B virus preS1/Myrcludex B binding in vivo; the NTCP-independent hepatic BA uptake machinery maintains a (slower) enterohepatic circulation of BAs, although it is occasionally insufficient to clear BAs from the circulation. (Hepatology 2015;62:207-219).

DOI: https://doi.org/10.1002/hep.27694

and hepatitis b virus pres1-binding in na(+) -taurocholate cotransporting polypeptide knockout mice. Hepatology, 62(1):207-219.
DOI: https://doi.org/10.1002/hep.27694

Impaired uptake of conjugated bile acids and Hepatitis B Virus preS1-binding in Na^+-taurocholate cotransporting polypeptide knockout mice

Davor Slijepcevic[1], Christina Kaufman[2,3], Catharina G.K. Wichers[4], Eduardo H. Gilglioni[1], Florian A. Lempp[2], Suzanne Duijst[1], Dirk R. de Waart[1], Ronald P.J. Oude Elferink[1], Walter Mier[3], Bruno Stieger[5], Ulrich Beuers[1], Stephan Urban[2,6] and Stan F.J. van de Graaf[1]

[1]Tytgat Institute for Liver and Intestinal Research & Department of Gastroenterology & Hepatology, AMC, Amsterdam, the Netherlands
[2]Department of Infectious Diseases, Molecular Virology, University Hospital Heidelberg, Germany
[3]Department of Nuclear Medicine, University Hospital Heidelberg, Germany
[4]Department of Molecular Cancer Research, Section Metabolic Diseases, University Medical Center Utrecht, the Netherlands
[5]Department of Clinical Pharmacology and Toxicology, University Hospital Zurich, Switzerland
[6]German Center for Infection Research, Heidelberg University, Germany

Correspondence to:

Stan van de Graaf

Meibergdreef 69-71

1105 BK Amsterdam

Phone number: 020-5668832

Fax number: 020-5669190

E-mail address: k.f.vandegraaf@amc.uva.nl

This article has been accepted for publication and undergone full peer review but has not been through the copyediting, typesetting, pagination and proofreading process which may lead to differences between this version and the Version of Record. Please cite this article as doi: 10.1002/hep.27694

Keywords

NTCP,

OATP,

Bile acid transport,

Myrcludex B,

Slc10a1-knockout mouse

List of abbreviations

BA	bile acid
NTCP	sodium taurocholate cotransporting polypeptide
OATP	organic anion transporting polypeptide
TCA	taurocholic acid
FXR	farnesoid X receptor
SHP	small heterodimer partner
HBV	hepatitis B virus
HDV	hepatitis D virus
L-protein	large surface protein
PMHs	primary mouse hepatocytes
NMDG	N-methyl-D-glucamine
HPLC	high pressure liquid chromatography
TαMCA	tauro-alpha-muricholic acid
TβMCA	tauro-beta-muricholic acid
TUDCA	tauroursodeoxycholic acid
TCDCA	taurochenodeoxycholic acid
TDCA	taurodeoxycholic acid

ωMCA	omega-muricholic acid
αMCA	alpha-muricholic acid
βMCA	beta-muricholic acid
CA	cholic acid
UDCA	ursodeoxycholic acid
CDCA	chenodeoxycholic acid
DCA	deoxycholic acid
ASBT	apical sodium-dependent bile acid transporter
OSTα/β	organic solute transporter alpha / beta
MRP2	multidrug resistance-associated protein 2
PET	positron emission tomography
SUV BW	Standardized uptake value body weight

Financial Support

SFJvdG is supported by the Netherlands Organization for Scientific Research (Vidi) and the European Research Council (Starting grant). SU received funding from the Deutsche Forschungsgemeinschaft (DFG, UR72 5-1) and the Deutsche Zentrum für Infektionskrankheiten/German Center for Infectious Diseases TTU Hepatitis (DZIF)

Acknowledgement

The authors gratefully acknowledge the excellent technical help of Karin Leotta and Max Sauter for the radiolabelling and the imaging experiments.

Disclosures

Stephan Urban is co-applicant and co-inventor on patents protecting HBV preS-derived lipopeptides (Myrcludex B) for the use as HBV/HDV entry inhibitors. The remaining authors disclose no conflicts.

Word count

4,944

Abstract

The Na^+-taurocholate cotransporting polypeptide (NTCP) mediates uptake of conjugated bile acids (BAs) and is localized at the basolateral membrane of hepatocytes. NTCP has recently been recognized as the receptor mediating hepatocyte-specific entry of Hepatitis B (HBV) and Hepatitis Delta viruses (HDV). Myrcludex B, a peptidic inhibitor of HBV entry, is assumed to specifically target NTCP. Here, we investigated BA transport and Myrcludex B binding in the first *Slc10a1*-knockout mouse model (*Slc10a1* encodes NTCP). Primary *Slc10a1*$^{-/-}$ hepatocytes showed absence of sodium-dependent taurocholic acid (TCA) uptake, whereas sodium-independent TCA uptake was unchanged. *In vivo*, this presented as a decreased serum BA clearance in all knockout mice. In a subset of mice, NTCP deficiency resulted in markedly elevated total serum BA concentrations, mainly composed of conjugated BAs. The hypercholanemic phenotype was rapidly triggered by a diet supplemented with UDCA. Biliary BA output remained intact, while fecal BA excretion was reduced in hypercholanemic *Slc10a1*$^{-/-}$ mice, explained by increased *Asbt* and *Ostα/β* expression. These mice further showed reduced *Asbt* expression in kidney and increased renal BA excretion. Hepatic uptake of conjugated BAs was potentially affected by downregulation of OATP1A1 and upregulation of OATP1A4. Furthermore, sodium-dependent TCA uptake was inhibited by Myrcludex B in wild-type hepatocytes, while *Slc10a1*$^{-/-}$ hepatocytes were insensitive to Myrcludex B. Finally, positron emission tomography showed a complete abrogation of hepatic binding of labelled Myrcludex B in *Slc10a1*$^{-/-}$ mice.

Conclusion: The *Slc10a1*-knockout mouse model supports the central role of NTCP in hepatic uptake of conjugated BAs and HBV preS1/Myrcludex B binding *in vivo*. The NTCP-independent hepatic BA uptake machinery maintains a (slower) enterohepatic circulation of BAs, although it is occasionally insufficient to clear the circulation from BAs.

During and after a meal, BAs are released into the small intestine, where they facilitate the absorption of dietary fat and fat-soluble vitamins (1). The majority of BAs are reabsorbed in the terminal ileum and transported back to the liver via the portal circulation. At the basolateral membranes of the hepatocytes, BAs are taken up from the portal circulation, are extruded across the canalicular hepatocyte membrane and transported to the gallbladder to complete the enterohepatic circulation (2). Conjugated BAs are transported across the basolateral hepatic membrane via a sodium-dependent pathway, mainly mediated by the sodium taurocholate cotransporting polypeptide (NTCP; gene name *SLC10A1*) (3, 4), and a sodium-independent pathway. The latter is likely mediated by members of the organic anion transporter superfamily (OATPs), which are also responsible for the hepatocellular uptake of unconjugated BAs (5, 6). NTCP is a liver-specific dimeric transmembrane glycoprotein (7) responsible for the majority of glycine/taurine-conjugated BA uptake in primary hepatocytes (4). Besides its role in BA homeostasis, NTCP is able to transport sulphated steroids, thyroid hormones and xenobiotics (8, 9). Reducing hepatocellular BA uptake is considered as a hepatic defence mechanism to prevent accumulation of potentially toxic BAs within hepatocytes. NTCP is regulated at the transcriptional level by cellular signalling pathways directly or indirectly involving farnesoid X receptor (FXR) and small heterodimer partner (SHP) (10). NTCP is strongly downregulated in conditions that could lead to hepatocellular BA overload, such as cholestasis (11). Recently, interest in NTCP activity and regulation and its contribution to BA homeostasis was boosted immensely when Li and co-workers identified NTCP as the functional cellular receptor permitting HBV and HDV to enter

primary human liver cells (12). Their findings were confirmed by others (13), who showed that HBV binding to NTCP is mediated by the myristoylated preS1-domain of the HBV large surface (L)-protein (14). NTCP-mediated virus entry is blocked by Myrcludex B, a synthetic preS1-lipopeptide derived from the HBV L-protein (15). The consequences of prolonged inhibition of NTCP-mediated BA transport *in vivo* are unknown. This is important to investigate, since Myrcludex B inhibits NTCP-mediated BA uptake at high concentrations (13). Here, we describe the first genetic knockout mouse model to study the consequences of prolonged and complete absence of NTCP. Our findings underscore that NTCP plays a pivotal role in hepatic uptake of conjugated BAs *in vivo* and is a crucial receptor for the myristoylated preS1-domain of the HBV L-protein.

Materials & methods

More detailed information about quantification of BAs, hepatocyte culture and TCA uptake *in vitro*, BA dynamics *in vivo*, Myrcludex imaging and on the methods described below is provided in the Supplementary Information.

Gene-targeting strategy and generation of Slc10a1$^{-/-}$ mice

Mice heterozygously lacking exon 1 of *Slc10a1* were generated by Lexicon Genetics Incorporated (The Woodlands, Texas, US), and obtained via Taconic (Hudson, NY, US). Detailed information on gene-targeting (Figure 1A) and mouse housing and feeding is provided as Supplementary Information. The study design and all protocols for animal care and handling were approved by the Institutional Animal Care and Use Committee of the University of Amsterdam.

RNA isolation, qRT-PCR and Western Blot analysis

Total RNA was isolated with TRIzol reagent (Invitrogen, Bleiswijk, The Netherlands). cDNA was synthesized from DNAse-treated total RNA with Oligo-dT$_{12-18}$ and Superscript II reverse transcriptase (Invitrogen). Quantitative real-time PCR (qRT-PCR) was carried out in a Roche Lightcycler 480 II instrument using SensiFAST SYBR No-ROX kit (Bioline, UK). Expression levels in each sample were normalized for the geometrical mean of two reference genes (Supplementary Information). Crude mouse liver membranes were isolated by ultracentrifugation and the pellets were resuspended in RIPA buffer (50 mM Tris-HCl pH 8.0, 150 mM NaCl, 1% (v/v) NP-40, 0.5% (w/v) Na-deoxycholate, 0.1% (w/v) SDS). Membrane proteins were separated on a

10% SDS-polyacrylamide electrophoresis gel, transferred to nitrocellulose and probed with primary antibodies as described in the Supplementary Information. Equal loading was ensured by reprobing the membrane with an anti-sodium/potassium ATPase antibody (kind gift of J. Koenderink, Nijmegen, the Netherlands) or with an anti-β-actin antibody (Abcam; ab8226).

Bile secretion and TCA elimination in vivo

Bile secretion in fasted *Slc10a1*$^{-/-}$ mice was investigated by performing gall bladder cannulation and bile collection for 30 minutes after distal ligation of the common bile duct (16). Bile flow was determined gravimetrically assuming a density of 1 g/mL for bile. Bile output was calculated as the product of the bile flow and the bile concentration in the second 10-minute collection period. After the 30 minutes depletion-phase, a single bolus of 150 µmol TCA / kg mouse (including a trace amount of tritium-labelled TCA) was administered intravenously in the tail vein in 100 µL 0.9% NaCl per 20 g mouse. A heating pad maintained body temperature at 37 °C. Blood samples (~30 µL) were collected 30 minutes before TCA administration and both blood and bile were collected at the indicated time points after TCA administration. Radioactivity in serum and bile was measured by liquid scintillation counting, and values are shown as a percentage of the total bolus (=100%).

Peptide synthesis, ^{68}Ga-labelling and PET-imaging

Myrcludex B-derived myristoylated HBV preS1 peptides were synthesized on a solid phase matrix using fluorenylmethoxycarbonyl/*t*-butyl (Fmoc/*t*Bu) chemistry, as previously described (17). A full description of Myrcludex B

synthesis is provided in the Supplementary Information. Peptides are depicted schematically in supplementary figure 4. For ^{68}Ga-labelling, 1000 µl [^{68}Ga]Ga^{3+} eluate, 20 µl of a 1 mM peptide solution in DMSO, 10 µl ascorbic acid solution (20% in H_2O) and 295 µl 2.5 M sodium acetate were mixed (pH 3.6) and heated at 90 °C for 15 minutes. The labelled peptide was purified using solid phase extraction (Thermo Scientific, Schwerte, Germany), eluted (ethanol), dried, dissolved in 60 µl DMSO and 240 µl of 0.9% NaCl was added. Mice were anesthetized with 1% sevoflurane (Abbott, Wiesbaden, Germany) and placed into an Inveon small animal PET scanner (Siemens, Knoxville, US). Investigators were blinded to mouse genotypes. A dynamic microPET was performed up to 60 min post-injection with ^{68}Ga-labelled peptides (6 to 27 MBq/animal in a 100 µl peptide solution in a tail vein).

Statistical analysis

Data are provided as the mean ± standard error of the mean. Differences between groups were analysed using 2-tailed Student's t-test. For serum and bile kinetics, half-time ($t_{½}$) and one-phase decay curves were calculated using Graphpad Prism 5. Statistical significance was considered at $p<0.05$.

Results

Generation of NTCP-deficient mice by targeted knockout of the *Slc10a1* gene

Homologous recombination leading to the deletion of exon 1 in the *Slc10a1* locus (figure 1A) on chromosome 12, with replacement of a β-galactosidase/puromycin resistance gene cassette in embryonic stem cells and generation of heterozygous knockout animals was performed by Lexicon. NTCP-deficient offspring showed normal Mendelian frequency and viability. They were fertile and showed no obvious anatomic abnormalities. PCR analysis identified the expected recombination by revealing the *Slc10a1* wild-type (412-bp) and targeted (624-bp) alleles in both male and female mice (figure 1B; primers are shown in supplementary table 1). Analysis of liver RNA revealed that the *Slc10a1* mRNA was totally absent in the knockout mice, and was reduced to 39.9 ± 8.7% and 43.1 ± 6.4% in male and female heterozygous mice, respectively, compared to wild-type mice (figure 1C). This suggests a lack of transcripts or an unstable *Slc10a1* product in knockout mice. Note that the primers encompass exon 4 of *Slc10a1*, which is not targeted by homologous recombination (see supplementary table 2). Furthermore, a glycosylated form of NTCP (~45-50 kDa; supplementary figure 1B) was detected in the liver homogenates of wild-type mice (n=3), but was undetectable in knockout mice, as shown by Western blot analysis (figure 1D). In heterozygous mice, the NTCP protein expression was approximately 90 ± 30% of the levels observed in wild-type mice (supplementary figure 1A), explaining the absence of any apparent phenotypic changes in those mice.

Lack of NTCP signal in immunofluorescent stainings of mouse liver confirmed the null phenotype (figure 1E).

Diminished TCA uptake and extremely high taurine-conjugated serum BA concentrations in adult *Slc10a1*$^{-/-}$ mice

To assess whether *Slc10a1*$^{-/-}$ mice lose sodium-dependent BA uptake, TCA transport was assessed in sandwich cultured primary mouse hepatocytes (PMHs) from wild-type and *Slc10a1*$^{-/-}$ mice. Since *Slc10a1* expression is rapidly downregulated in primary hepatocyte cultures (18, 19), the TCA uptake assay was performed 3 hours after PMH seeding. Uptake increases in a linear fashion within at least 60 seconds (data not shown). Sodium-dependent TCA uptake of wild-type PMH was 66.0 ± 7.1 pmol/min, which decreased to 29.2 ± 1.7 pmol/min following replacement of Na^+ with NMDG (Figure 2A). This sodium-dependent TCA uptake was completely absent in *Slc10a1*$^{-/-}$ PMHs, which showed similar TCA uptake as wild-type mice under sodium-free conditions (24.3 ± 3.6 pmol/min). The presence of 1 μM Myrcludex B abrogated sodium-dependent TCA uptake in wild-type PMHs, as shown previously (13), but had no effect on TCA uptake under sodium-free conditions. In *Slc10a1*$^{-/-}$ PMHs, TCA uptake remained at similar levels in the sodium-dependent as well as sodium-free conditions, and this was unaffected by the addition of 1 μM Myrcludex B.

To investigate whether NTCP affects BA homeostasis, total serum BA concentrations and different BA species were measured in wild-type and *Slc10a1*$^{-/-}$ mice fed a standard diet. A subpopulation of NTCP-deficient mice

had significantly elevated total serum BA levels, reaching millimolar concentrations (figure 2B). No obvious gender differences were observed for this phenotype. Total serum BA levels were in the normal range for both wild-type and heterozygous mice (range 1-21 μmol/L), and only wild-type mice were used for further comparisons. Notably, the majority of *Slc10a1*$^{-/-}$ mice (60-75%) had normal serum BA concentrations, despite complete lack of NTCP protein. Hypercholanemia during NTCP deficiency was defined as total serum BA levels >20 μmol/L. Both hypercholanemia and normocholanemia in *Slc10a1*$^{-/-}$ mice were preserved during the backcross to C57Bl/6J (from 50% genetically similar to 129/SvEv to >98% similar to C57Bl/6J), excluding effects of different mouse strain backgrounds. Next, the serum concentrations of individual BA species was determined by HPLC. *Slc10a1*$^{-/-}$ mice with high serum BA concentrations had significant increases in taurocholic acid (TCA), tauro-α-muricholic acid (TαMCA) and tauro-β-muricholic acid (TβMCA) (figure 2C), which were 1673 ± 840.1 μmol/L, 107.9 ± 63.1 and 439.8 ± 214.3 μmol/L, respectively. NTCP deficiency caused a relative mild increase in unconjugated BAs, only in mice with high serum BA concentrations, which was caused by an increase of deoxycholic acid to 87.4 ± 65.3 μmol/L (figure 2D). Glycine-conjugated species were below the detection limit (0.125 μmol/L) in all mice, thus they were not included in our results. *Slc10a1*$^{-/-}$ mice with high serum BA concentrations have a shift towards increased conjugated BA species (87 ± 12% of total; as to 59.8 ± 12% in wild-type mice) (figure 2E), whereas this shift was not observed in *Slc10a1*$^{-/-}$ mice with physiological BA concentrations (51.7 ± 10% of total).

Phenotype characteristics of *Slc10a1*$^{-/-}$ mice

Heterozygous mice carrying one intact *Slc10a1* allele were indistinguishable from wild-type littermates. *Slc10a1*$^{-/-}$ mice were phenotypically very similar to their littermates, except that the mice (in both the male and female group) had reduced body weights directly post-weaning (day 21) compared to littermates and this difference was also present at 2 months of age (table 1). The body weights were inversely correlated with total serum BA levels (figure 2F), and the hypercholanemic knockout mice had a strongly reduced body weight. Liver morphology appeared macroscopically normal, and the ratios of liver weight to body weight were unaffected. Serum concentrations of conjugated bilirubin were moderately increased from 2.6 ± 0.6 µmol/L in wild-type mice to 31.4 ± 8.0 µmol/L in hypercholanemic knockout mice, whereas normocholanemic knockout mice did not show any elevations in conjugated bilirubin levels. Furthermore, no significant differences were found in aspartate transaminase and alanine transaminase between wild-type and hypercholanemic *Slc10a1*$^{-/-}$ mice (supplementary table 3). Alkaline phosphatase increased from 22.0 ± 6.2 U/L in wild-type mice to 219.1 ± 38.8 U/L in hypercholanemic knockout mice. These biochemical values are not indicative of extensive hepatobiliary damage as ~10 to 20 times higher serum levels of bilirubin and alanine transaminase are detected in severely cholestatic rodents, for instance bile duct-ligated mice (20). Examination of hematoxylin- and eosin-stained liver sections for all genotypes revealed no overt abnormalities. In particular, no signs of cholestasis, inflammation or hepatocellular damage were observed in *Slc10a1*$^{-/-}$ mice (supplementary figure 2).

Normocholanemic *Slc10a1*$^{-/-}$ mice fed a 0.1% ursodeoxycholic acid diet rapidly develop extremely high serum BA concentrations

To challenge the hepatic BA uptake machinery during NTCP deficiency, both young and adult wild-type and *Slc10a1*$^{-/-}$ mice were fed for 4 to 8 days with 0.1% UDCA, with the rationale to increase the amount of BAs reaching the portal circulation that need to be handled by the liver. Under this condition, young *Slc10a1*$^{-/-}$ mice showed extremely high serum BA levels, which was attributed to a significant increase in conjugated BAs, mainly TCA and TβMCA (figure 3A), but also unconjugated species tended to be elevated in a subset of mice (figure 3B). Experiments were repeated with adult mice, and BA levels were measured before start of UDCA-supplementation. After 1 week of 0.1% UDCA-supplementation, total serum BA concentrations in adult *Slc10a1*$^{-/-}$ mice significantly increased from 514.4 ± 309.1 µmol/L to 2528 ± 792.7; versus 3.4 ± 1.4 µmol/L in wild-type mice fed UCDA (figure 3C). Two knockout mice could not be forced into hypercholanemia post-UDCA-supplementation, having comparable BA levels as wild-type mice. Two out of eight *Slc10a1*$^{-/-}$ mice were already hypercholanemic pre-UDCA-supplementation and remained extremely hypercholanemic. These findings suggest that the NTCP-independent hepatic BA uptake machinery operates close to its maximum capacity in *Slc10a1*$^{-/-}$ mice and can easily be saturated.

Delayed serum TCA elimination and biliary excretion in *Slc10a1*$^{-/-}$ mice

To examine the contribution of NTCP to (conjugated) BA kinetics *in vivo*, we investigated the clearance of conjugated BAs from serum into bile by

intravenous administration of TCA in wild-type and both normocholanemic and hypercholanemic *Slc10a1*$^{-/-}$ mice. Serum TCA elimination half-time significantly increased from 1.5-minutes (CI 1.2 ± 2.3) in wild-type to 5.3-minutes (CI 3.9 ± 7.9) in normocholanemic *Slc10a1*$^{-/-}$ mice (figure 4A). Also, biliary excretion of TCA was evidently delayed in normocholanemic *Slc10a1*$^{-/-}$ mice compared to wild-type mice (figure 4B). The high-dose of TCA proved to be lethal in hypercholanemic *Slc10a1*$^{-/-}$ mice shortly after injection. To assess systemic BA clearance during hypercholanemia, total serum BA concentrations were determined in time in these mice after gall bladder cannulation, without prior TCA administration. We observed a markedly delayed serum BA clearance ($t_{½}$ >40 min; figure 4C).

Biliary, fecal and renal BA excretion during NTCP deficiency

General BA excretion during NTCP deficiency was investigated by collecting bile during a 30-minute period. At every time point after gall bladder cannulation, no significant changes in bile flow were observed between wild-type and normocholanemic *Slc10a1*$^{-/-}$ mice (figure 5A), while hypercholanemic *Slc10a1*$^{-/-}$ mice showed a trend towards slightly decreased bile flow (p=0.38). Biliary excretion of BAs was determined in the second 10-minute period after gall bladder cannulation, and no significant differences were measured between wild-type mice, normocholanemic and hypercholanemic *Slc10a1*$^{-/-}$ mice (figure 5B). Hence, biliary excretion of BAs appears unaffected by NTCP deficiency.

To gain insight into BA excretion routes during NTCP deficiency, fecal and urinary BA levels were measured, together with ileal and renal mRNA expression of major BA transporters. Total fecal BA excretion significantly decreased to 0.6 ± 0.1 µmol/day/100g BW during hypercholanemia (figure 5C) compared to 2.8 ± 0.9 and 3.0 ± 0.8 µmol/day/100g BW in wild-type and normocholanemic *Slc10a1*$^{-/-}$ mice. Decreased fecal BA excretion corresponded with elevated mRNA expression of ileal *Asbt* (p=0.09), *Ostα* and *Ostβ* (figure 5D). Very high urinary BA concentrations were measured during hypercholanemia (figure 5E). Urinary BAs were mainly taurine-conjugated muricholates and cholate (data not shown). Decreased expression of renal *Asbt* to ~30% of wild-type and normocholanemic mice, corresponded with increased renal BA excretion (figure 5F). Notably, renal expression of both the basolateral bi-directional BA transporter *Ostα/β* and the apical BA extrusion transporter *Mrp2* was significantly increased, suggesting that also tubular BA transport towards the lumen might contribute to urinary BA excretion.

Hepatic expression of BA-transporting OATP family members

We investigated whether the basolateral hepatic BA transporters of the OATP family (21) or the OSTα/β family compensate for the loss of NTCP, possibly explaining the normocholanemia in a subset of the *Slc10a1*$^{-/-}$ mice by restoring (conjugated) BA transport capacity. To this end, hepatic gene expression levels of mouse *Slco1a1* (*Oatp1a1*), *Slco1a4* (*Oatp1a4*), *Slco1b2* (*Oatp1b2*), and *Slc51a* (*Ostα*) were analyzed by qRT-PCR (figure 6A). Messenger RNA expression levels of all tested *Oatp* family members were

unaffected in normocholanemic *Slc10a1*$^{-/-}$ mice and *Ostα* mRNA was undetectable in all *Slc10a1*$^{-/-}$ mice (not shown). During hypercholanemia, *Oatp1b2* and *Oatp1a1* mRNA levels decreased to respectively 36 ± 14% and 40 ± 11% of wild-type levels, and the relative change was not caused by gender differences. On the other hand, *Oatp1a4* mRNA significantly increased to 189% ± 30%. To determine the gene expression of *Oatp* family members in response to BA supplementation, wild-type and hypercholanemic *Slc10a1*$^{-/-}$ mice were analyzed post-UDCA-supplementation. *Oatp* family members were regulated in the same pattern as during spontaneous hypercholanemia (supplementary figure 3). Consistent with the mRNA expression pattern, OATP1A1 protein was virtually lost during hypercholanemia, while OATP1A4 protein was significantly upregulated (in both genders, figure 6B). Notably, OATP1A1 (male predominant) and OATP1A4 (female predominant) had gender-regulated protein expression levels. In contrast, *Oatp1b2* mRNA and protein expression did not correlate, as OATP1B2 protein expression remained stable during NTCP deficiency. These results were opposite to the gene expression levels, suggesting that post-transcriptonal regulation occurs, which has been described for Oatp isoforms by Rippin et al (19).

Abrogation of Myrcludex B accumulation in the livers of *Slc10a1*$^{-/-}$ mice

We evaluated the distribution of radiolabelled Myrcludex B-derived lipopeptide after intravenous injection in wild-type, heterozygous and *Slc10a1*$^{-/-}$ mice. To this end, we developed peptides suitable for PET-imaging containing either the Myrcludex B sequence (^{68}Ga-WT peptide) or a mutation in the residues required for binding (^{68}Ga-control peptide). The functionality of the peptides

for liver targeting was confirmed in wild-type mice (supplementary figure 4). As previously shown (22), Myrcludex B-derived peptides specifically enrich in the liver of wild-type mice, while mutations in the essential receptor binding residues of the peptide lead to a loss of hepatocyte binding. Crucially, livers of *Slc10a1*$^{-/-}$ mice had virtually no accumulation of radiolabelled Myrcludex B signal and livers of heterozygous mice have reduced accumulation (60-70% compared to wild-type) (figure 7A). The distribution pattern of the ^{68}Ga-WT peptide in *Slc10a1*$^{-/-}$ mice was identical to the pattern observed in wild-type mice injected with the ^{68}Ga-control peptide. Within minutes, the WT peptide enriched in the liver of wild-type mice, whereas in *Slc10a1*$^{-/-}$ mice the detected signal within the liver remained at a constantly low level, which represents the blood flow through the organ (figure 7B; left panel). Non-liver bound peptide in *Slc10a1*$^{-/-}$ mice accumulated in the kidneys (figure 7B; right panel), where it was eliminated from the circulation. No gender differences were observed. Thus, *Slc10a1*$^{-/-}$ mice lost the ability to bind Myrcludex B in the liver.

Discussion

The present study shows the first characterization of *Slc10a1*-knockout mice and illustrates the importance of this liver-specific transporter for the hepatic uptake of conjugated BAs and as a receptor for Myrcludex B, a synthetic preS1-lipopeptide derived from the HBV L-protein.

We describe the consequences of complete and prolonged absence of NTCP functionality *in vivo*. Recently, a 5-year-old patient was described with homozygosity for NTCP p.Arg252His, a mutation that strongly affects NTCP targeting to the plasma membrane (23). This girl showed persistent hypercholanemia without any sign of liver injury or pruritus. Other NTCP genetic variants were previously described that result in impaired BA transport capacity (e.g. p.Ser267Phe (24)), but no phenotype is yet described to associate with these variants. Our data of *Slc10a1*$^{-/-}$ mice support these findings, as 30-35% of the adult mice have markedly elevated total BA levels in serum and strongly reduced body weight. In line with the function of NTCP as a sodium-dependent transporter of mainly conjugated BAs, these mice mainly show serum accumulation of taurine-conjugated BAs. Despite the reduced body weights and a strongly reduced capacity to remove conjugated BAs from the circulation in *Slc10a1*$^{-/-}$ mice, no overt liver damage was observed. Moderate elevations in serum ALP and bilirubin levels were only present in hypercholanemic *Slc10a1*$^{-/-}$ mice and many *Slc10a1*$^{-/-}$ mice were normocholanemic. This relatively mild phenotype is in line with that of the single NTCP-deficient patient described to date. The distribution of the mice across these two groups (normocholanemic versus hypercholanemic)

persisted over all generations while the mice were backcrossed to C57Bl/6J genetic background. We have also observed temporal normalization of the serum BA concentration, as well as mature onset of hypercholanemia, further excluding mouse genotype/strain effects.

We hypothesize that the sodium-independent hepatic uptake machinery is able to sustain the enterohepatic cycle of (conjugated) BAs, but in a subset of *Slc10a1*$^{-/-}$ mice the flux of BAs can (temporarily) exceed the maximum capacity of the liver to effectively clear the portal circulation from BAs. In line with this hypothesis is our finding that *Slc10a1*$^{-/-}$ mice accumulate high amounts of BAs in the circulation if they are challenged with 0.1% UDCA, and this hypercholanemia is inducible in *Slc10a1*$^{-/-}$ mice with normal or minimally elevated serum BA concentrations. Notably, this increase of serum BAs included multiple (mostly conjugated) BA species, and not only (T)UDCA, which is in line with a saturated uptake machinery. Furthermore, these findings suggest that the enterohepatic circulation is still sustained, as UDCA is conjugated and also slightly increased levels of unconjugated BAs were measured, including CA and DCA. As DCA itself seems to be a poor substrate for NTCP (25, 26), increased serum DCA could point to a competitive inhibition of the OATP family members by conjugated BAs, combined with the loss of OATP1A1 protein. A mild conjugated hyperbilirubinemia was observed in hypercholanemic *Slc10a1*$^{-/-}$ mice, without evident cholestatic damage. This observation could support the hypothesis of competitive inhibition of OATP isoforms, as the total *Oatp1a/1b*-knockout mouse showed a 40-fold increase of serum conjugated bilirubin (27).

The hypercholanemic *Slc10a1*$^{-/-}$ mice display interesting changes in expression of hepatic, ileal and renal BA transporters. Also notable is that no changes in *Oatp* mRNA levels are detected in normocholanemic *Slc10a1*$^{-/-}$ mice, suggesting that compensatory upregulation of these transporters is not occurring in NTCP-deficient mice. In line with this finding, *in vitro* TCA uptake of PMHs under sodium-free conditions is similar between wild-type and normocholanemic *Slc10a1*$^{-/-}$ mice. In contrast, *Oatp1a1* mRNA and protein levels decreased in hypercholanemic *Slc10a1*$^{-/-}$ mice, whereas *Oatp1a4* mRNA and protein levels slightly increased. Although it is presently unclear if the changes in OATP expression are due to or a cause of the hypercholanemic phenotype, absence of OATP1A1 could further reduce the hepatic uptake capacity for conjugated BAs (5), contributing to the hypercholanemia. In contrast, upregulation of OATP1A4 could contribute to systemic BA clearance during NTCP deficiency. Fecal BA excretion does certainly not provide a likely compensatory mechanism to reduce hypercholanemia during NTCP deficiency, considering the enhanced *Asbt* expression and strongly reduced fecal BA excretion. On the other hand, enhanced renal BA excretion is the most likely route of BA elimination when hepatic BA uptake capacity reaches its maximum, thereby attenuating the circulatory BA overload. This could be mechanistically confirmed by a reduced renal *Asbt* expression. Interestingly, renal *Ostα/β* and *Mrp2* mRNA expression were increased, possibly allowing excretion of BAs into the ductular lumen, as OSTα/β has bi-directional transport properties. This hypothesis as well as the

underlying mechanisms for sensing changes in BA dynamics and modulating transporter expression will require further investigation.

Recently, NTCP was identified as the receptor for HBV/HDV entry, using a proteomic approach to identify proteins that bind the preS1 domain of the HBV L-protein (12). This finding could explain many of the characteristics of HBV, including its specificity to infect hepatocytes (hepatotropism), as these are the only cells that express NTCP. The rapid loss of infectability of primary hepatocytes and the total lack of virus binding in virtually all cell lines could now be linked to downregulation of NTCP upon isolation of primary cells and absence of NTCP expression in all cell lines except differentiated HepaRG cells. The myristoylated preS1 subdomain of the HBV L-protein specifically binds to the liver in many (also non-HBV-susceptible) animals, including mice (22). This exclusive liver targeting makes Myrcludex B a very interesting potential drug with high hepatocyte specificity. Using the *Slc10a1*-knockout model, we here show that NTCP is essential for Myrcludex B binding *in vivo*, with a total lack of liver association in *Slc10a1*$^{-/-}$ mice, indicating that association with NTCP mediates the liver-specificity of Myrcludex B and supporting a role for NTCP in HBV hepatotropism.

Taken together, this report is the first to describe and characterize a murine *Slc10a1*-knockout model in order to better understand the physiological relevance of this BA transporter. Data presented in this study show the importance of NTCP for sodium-dependent hepatic BA uptake *in vivo* and for hepatic binding of Myrcludex B, a peptidic inhibitor of HBV entry.

References

1. Hofmann AF. Bile Acids: The Good, the Bad, and the Ugly. News Physiol Sci 1999;14:24-29.

2. Meier PJ, Stieger B. Bile salt transporters. Annu Rev Physiol 2002;64:635-661.

3. Hagenbuch B, Stieger B, Foguet M, Lubbert H, Meier PJ. Functional expression cloning and characterization of the hepatocyte Na^+-bile acid cotransport system. Proc Natl Acad Sci U S A 1991;88:10629-10633.

4. Stieger B. The role of the sodium-taurocholate cotransporting polypeptide (NTCP) and of the bile salt export pump (BSEP) in physiology and pathophysiology of bile formation. Handb Exp Pharmacol 2011:205-259.

5. Jacquemin E, Hagenbuch B, Stieger B, Wolkoff AW, Meier PJ. Expression cloning of a rat liver Na^+-independent organic anion transporter. Proc Natl Acad Sci U S A 1994;91:133-137.

6. Csanaky IL, Lu H, Zhang Y, Ogura K, Choudhuri S, Klaassen CD. Organic anion-transporting polypeptide 1b2 (Oatp1b2) is important for the hepatic uptake of unconjugated bile acids: Studies in Oatp1b2-null mice. Hepatology 2011;53:272-281.

7. Bijsmans IT, Bouwmeester RA, Geyer J, Faber KN, van de Graaf SF. Homo- and heterodimeric architecture of the human liver Na^+-dependent taurocholate cotransporting protein NTCP. Biochem J 2012;441(3):1007-15.

8. Kim RB, Leake B, Cvetkovic M, Roden MM, Nadeau J, Walubo A, Wilkinson GR. Modulation by drugs of human hepatic sodium-dependent bile acid transporter (sodium taurocholate cotransporting polypeptide) activity. J Pharmacol Exp Ther 1999;291:1204-1209.

9. Visser WE, Wong WS, van Mullem AA, Friesema EC, Geyer J, Visser TJ. Study of the transport of thyroid hormone by transporters of the SLC10 family. Mol Cell Endocrinol 2010;315:138-145.

10. Dawson PA, Lan T, Rao A. Bile acid transporters. J Lipid Res 2009;50:2340-2357.

11. Gartung C, Ananthanarayanan M, Rahman MA, Schuele S, Nundy S, Soroka CJ, Stolz A, et al. Down-regulation of expression and function of the rat liver Na^+-bile acid cotransporter in extrahepatic cholestasis. Gastroenterology 1996;110:199-209.

12. Yan H, Zhong G, Xu G, He W, Jing Z, Gao Z, Huang Y, et al. Sodium taurocholate cotransporting polypeptide is a functional receptor for human hepatitis B and D virus. Elife 2012;1:e00049.

13. Ni Y, Lempp FA, Mehrle S, Nkongolo S, Kaufman C, Falth M, Stindt J, et al. Hepatitis B and D viruses exploit sodium taurocholate co-transporting polypeptide for species-specific entry into hepatocytes. Gastroenterology 2014;146:1070-1083.

14. Meier A, Mehrle S, Weiss TS, Mier W, Urban S. Myristoylated PreS1-domain of the hepatitis B virus L-protein mediates specific binding to differentiated hepatocytes. Hepatology 2013;58:31-42.

15. Schulze A, Schieck A, Ni Y, Mier W, Urban S. Fine mapping of pre-S sequence requirements for hepatitis B virus large envelope protein-mediated receptor interaction. J Virol 2010;84:1989-2000.

16. Oude Elferink RP, Ottenhoff R, van Wijland M, Smit JJ, Schinkel AH, Groen AK. Regulation of biliary lipid secretion by mdr2 P-glycoprotein in the mouse. J Clin Invest 1995;95:31-38.

17. Schieck A, Müller T, Schulze A, Haberkorn U, Urban S, Mier W. Solid-phase synthesis of the lipopeptide Myr-HBVpreS/2-78, a hepatitis B virus entry inhibitor. Molecules 2010;15:4773-4783.

18. Liang D, Hagenbuch B, Stieger B, Meier PJ. Parallel decrease of Na^+-taurocholate cotransport and its encoding mRNA in primary cultures of rat hepatocytes. Hepatology 1993;18:1162-1166.

19. Rippin SJ, Hagenbuch B, Meier PJ, Stieger B. Cholestatic expression pattern of sinusoidal and canalicular organic anion transport systems in primary cultured rat hepatocytes. Hepatology 2001;33:776-782.

20. Wagner M, Halilbasic E, Marschall HU, Zollner G, Fickert P, Langner C, Zatloukal K, et al. CAR and PXR agonists stimulate hepatic bile acid and bilirubin detoxification and elimination pathways in mice. Hepatology 2005;42:420-430.

21. Hagenbuch B, Meier PJ. The superfamily of organic anion transporting polypeptides. Biochim Biophys Acta 2003;1609:1-18.

22. Schieck A, Schulze A, Gahler C, Muller T, Haberkorn U, Alexandrov A, Urban S, et al. Hepatitis B virus hepatotropism is mediated by specific receptor recognition in the liver and not restricted to susceptible hosts. Hepatology 2013;58:43-53.

23. Vaz FM, Paulusma CC, Huidekoper H, de Ru M, Lim C, Koster J, Ho-Mok K, et al. Sodium taurocholate cotransporting polypeptide (SLC10A1) deficiency: Conjugated hypercholanemia without a clear clinical phenotype. Hepatology 2014 May 28 [in press].

24. Pan W, Song IS, Shin HJ, Kim MH, Choi YL, Lim SJ, Kim WY, et al. Genetic polymorphisms in Na^+-taurocholate co-transporting polypeptide

(NTCP) and ileal apical sodium-dependent bile acid transporter (ASBT) and ethnic comparisons of functional variants of NTCP among Asian populations. Xenobiotica 2011;41:501-510.

25. van der Velden LM, Golynskiy MV, Bijsmans IT, van Mil SW, Klomp LW, Merkx M, van de Graaf SF. Monitoring bile acid transport in single living cells using a genetically encoded FRET sensor. Hepatology 2013 Feb;57(2):740-52.

26. Hagenbuch B, Meier PJ. Molecular cloning, chromosomal localization, and functional characterization of a human liver Na^+-bile acid cotransporter. J Clin Invest 1994;93:1326-1331.

27. van de Steeg E, Wagenaar E, van der Kruijssen CM, Burggraaff JE, de Waart DR, Elferink RP, Kenworthy KE, et al. Organic anion transporting polypeptide 1a/1b-knockout mice provide insights into hepatic handling of bilirubin, bile acids, and drugs. J Clin Invest 2010;120:2942-2952.

Legends

Figure 1: (a) Conventional knockout of *Slc10a1* in mouse ES cells by homologous recombination. A schematic representation of the mouse *Slc10a1* gene. Exon 1 was replaced by the β-galactosidase/puromycin (βgeo/puro) selection cassette located in the targeting vector (pKOS 73). Primers of the wild-type allele (wt-fw and wt-rv) and primers of the targeted allele (mut-fw and mut-rv) are shown. (b) Genomic DNA was isolated for genotyping of the offspring mice. PCR analysis detected fragments of the *Slc10a1* wild-type (412-bp) and targeted (624-bp) alleles. Homozygous wild-type (+/+) mice, as well as heterozygous (+/-) or homozygous knockout (-/-) male and female mice are shown. All PCR products were separated by 1.0% agarose gel electrophoresis. (c) *Slc10a1* mRNA expression in female and male wild-type (WT), heterozygous (HET) and *Slc10a1*$^{-/-}$ (KO) mouse livers, analyzed by qRT-PCR. *Slc10a1* expression values were calculated relative to the geometric mean of *Rplp0* and *Tbp* and normalized to male wild-type mice (set at 1.0). Data are represented as mean ± S.E.M. from 6-7 male (light grey) or female mice (dark grey). Asterisk indicates p-value below 0.05. (d) NTCP protein levels (~45-50 kDa) in liver plasma membranes of WT and KO male mice (n=3), analyzed by Western blot. Equal volumes of protein were loaded, as confirmed by the sodium/potassium ATPase (~90 kDa). (e) Immunofluorescent NTCP staining in WT and KO fresh frozen liver tissue. Scale bar is 40 µm.

Figure 2: (A) TCA uptake assay in primary hepatocytes of wild-type (WT) and *Slc10a1*$^{-/-}$ (KO) mice. TCA uptake was performed after pre-incubation for 30

minutes in sodium-containing buffer (Na, black bar), sodium-free buffer (NMDG, light grey bar), sodium-containing buffer plus 1 μM Myrcludex B (Na + Myr B, dark grey bar) and sodium-free buffer plus 1 μM Myrcludex B (NMDG + Myr B, white bar). Bars represent the mean ± S.E.M. for 2 independent experiments, each performed in triplicate. Asterisk indicates p-value below 0.05. (B) Total serum BA concentrations in male and female wild-type (WT) and *Slc10a1*$^{-/-}$ (KO) mice. Data are given as mean ± S.E.M on a ^{10}log scale for 7-16 mice in each group, quantified using the total BA assay. Serum composition of (C) conjugated and (D) unconjugated BA species as quantified using HPLC. Wild-type (white bars), *Slc10a1*$^{-/-}$ mice with normal (light grey bars), and *Slc10a1*$^{-/-}$ mice with high serum BA concentrations (dark grey bars) are shown. Conjugated BAs (C-BA) concentrations are the sum of TαMCA, TβMCA, TUDCA, TCA, TCDCA and TDCA. Unconjugated BAs (U-BA) concentrations are the sum of ωMCA, αMCA, βMCA, CA, UDCA, CDCA and DCA. Data are given as mean ± S.E.M on a ^{10}log scale for 3-6 mice in each group. Asterisk indicates p-value below 0.05 (compared to wild-type levels). (E) Serum BA composition of wild-type, *Slc10a1*$^{-/-}$ mice with normal, and KO mice high serum BA concentrations. Conjugated BA (dark grey) and unconjugated BA (light grey) species are shown as a percentage of total, as quantified using HPLC. (F) Total serum BA levels in relation to body weights of WT (open dots) and KO (black dots) 8-week-old mice (n=11-14).

Figure 3: Effects of BA supplementation on serum BA concentrations. After 4 days of 0.1% UDCA-supplementation, serum composition of (A) conjugated and (B) unconjugated BA species was measured in 5-week-old wild-type

(open dots) and *Slc10a1*$^{-/-}$ mice (black dots). Data are given as a scatter plot on a ^{10}log scale from 5 mice in each group. Asterisk indicates p-value below 0.05. (C) Total serum BA levels were measured before starting 0.1% UDCA-supplementation (pre-UDCA), and after 1 week (post-UDCA) in 8-10-week-old *Slc10a1*$^{-/-}$ mice (black dots). As a control total serum BA levels of wild-type mice (open dots) were measured after 0.1% UDCA-supplementation. Data are given on a ^{10}log scale from 4 wild-type and 8 *Slc10a1*$^{-/-}$ mice.

Figure 4: (A) *In vivo* serum TCA clearance and (B) cumulative biliary excretion in wild-type (open dots) and normocholanemic (black dots) *Slc10a1*$^{-/-}$ mice. TCA kinetics after an intravenous TCA bolus (150 µmol/kg BW) are given as a percentage of the whole bolus (=100%). Serum and bile kinetics are given as the mean ± S.E.M. (2 - 40 minutes post-injection, n=5). Mice were considered normocholanemic if total BA concentration was <20 µM before the start of the experiment. Cross symbol indicates death. (C) Total serum BA (TBA) clearance during hypercholanemia. TBA concentrations from 4 hypercholanemic *Slc10a1*$^{-/-}$ mice are given relative to the concentration at the start of gall bladder cannulation (set at 100%).

Figure 5: Effects of NTCP deficiency on the enterohepatic circulation. Bile was collected for 30 minutes after gall bladder cannulation and ligation of the common bile duct. (A) Bile flow (µL/min/100g BW) is shown during this period for wild-type (open dots), normocholanemic (black dots) and hypercholanemic (black triangles) *Slc10a1*$^{-/-}$ mice. (B) Bile acid output (nmol/min/100g BW)

during the 10 - 20 minute collection period for wild-type (white bar), normocholanemic *Slc10a1*$^{-/-}$ (light grey bar) and hypercholanemic *Slc10a1*$^{-/-}$ mice (dark grey bar). Data is given as mean ± S.E.M. (n=8-12). (C) Total fecal BA excretion (µmol/24h/kg BW) and (D) relative mRNA expression of BA transporters in the distal ileum for wild-type mice (white bars), *Slc10a1*$^{-/-}$ mice with low (light grey bars) and high (dark grey bars) serum BA concentrations, using the geometric mean of control genes *Hprt* and *Ppib*. (E) Urinary BA concentrations (µM) and (F) relative mRNA expression of renal BA transporters for wild-type (white bars), *Slc10a1*$^{-/-}$ mice with low (light grey bars) and high (dark grey bars) serum BA concentrations, using the geometric mean of control genes *Rplp0* and *Hprt*. Data (in C-F) is given as mean ± S.E.M. (n=4-6) from 6-8 week-old mice. Asterisk indicates p-value below 0.05 (compared to wild-type levels).

Figure 6: (A) *Oatp* mRNA expression as determined by RT-qPCR. Relative mRNA expression levels were calculated for wild-type mice (white bars), *Slc10a1*$^{-/-}$ mice with low (light grey bars) and high (dark grey bars) serum BA concentrations using the geometric mean of control genes *Rplp0* and *Tbp*. Both sexes were pooled equally. Values are given as mean ± S.E.M. for 4-6 mice per group. (B) Western blot analysis of the OATP1B2 (~80 kDa), OATP1A1 and OATP1A4 (both ~85 kDa) proteins. Protein expression levels were determined relative to the sodium/potassium ATPase (~90 kDa) and values are given as mean ± S.E.M. for 4-5 mice per group. Asterisk indicates p-value below 0.05 (compared to wild-type levels).

Figure 7: Myrcludex B-derived peptide binding assessed by microPET. (A) Female wild-type (+/+, first panel), heterozygous (+/-, second panel) and homozygous *Slc10a1*$^{-/-}$ (-/-, third panel) mice were imaged post-injection of ^{68}Ga-WT peptide or ^{68}Ga-control peptide (fourth panel). Top: Uncorrected planar projection, bottom: coronal PET section. (B) Time activity curves of ^{68}Ga-WT peptide (as SUV BW) in liver and kidney of wild-type (black line with dots), heterozygous (blue line with squares) and *Slc10a1*$^{-/-}$ (red line with triangles) male mice during 60 minutes post-injection.

Figure 1

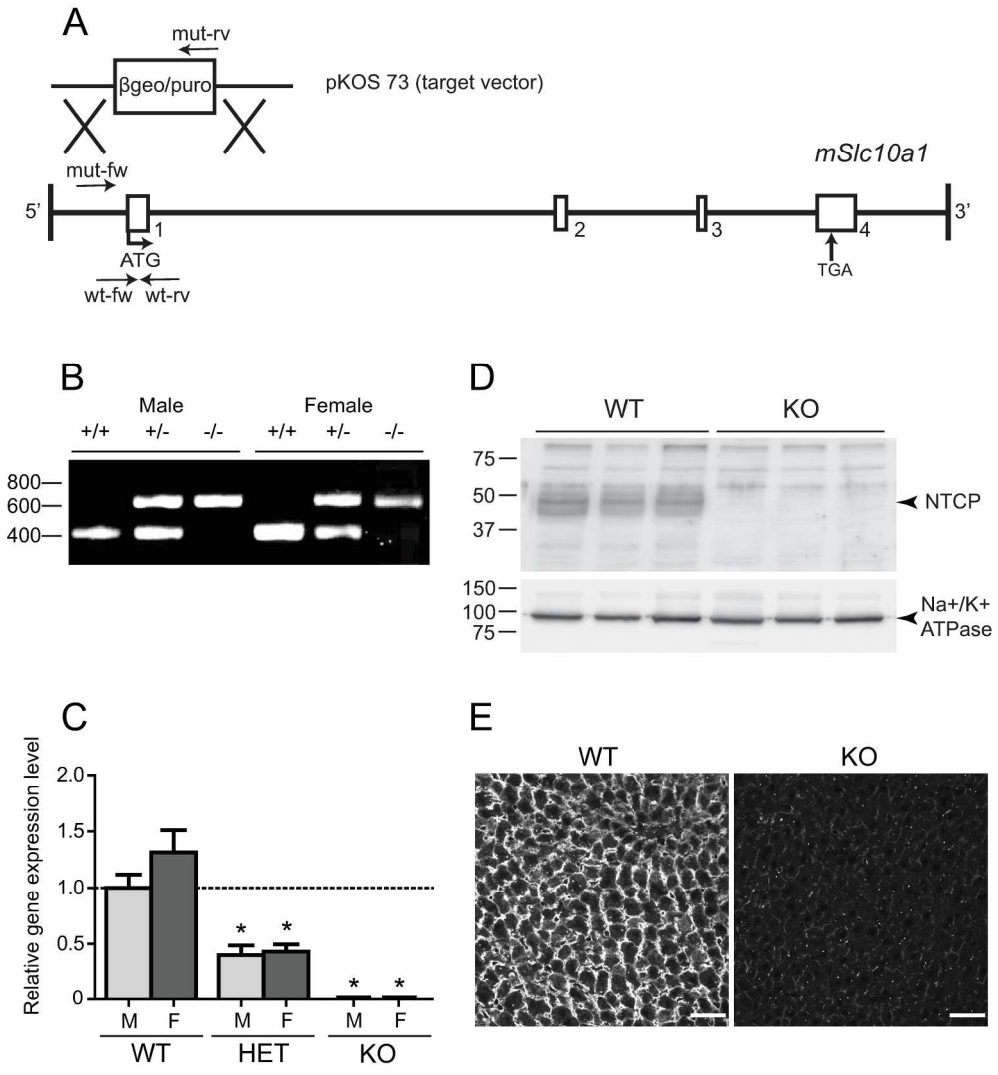

238x276mm (300 x 300 DPI)

Figure 2

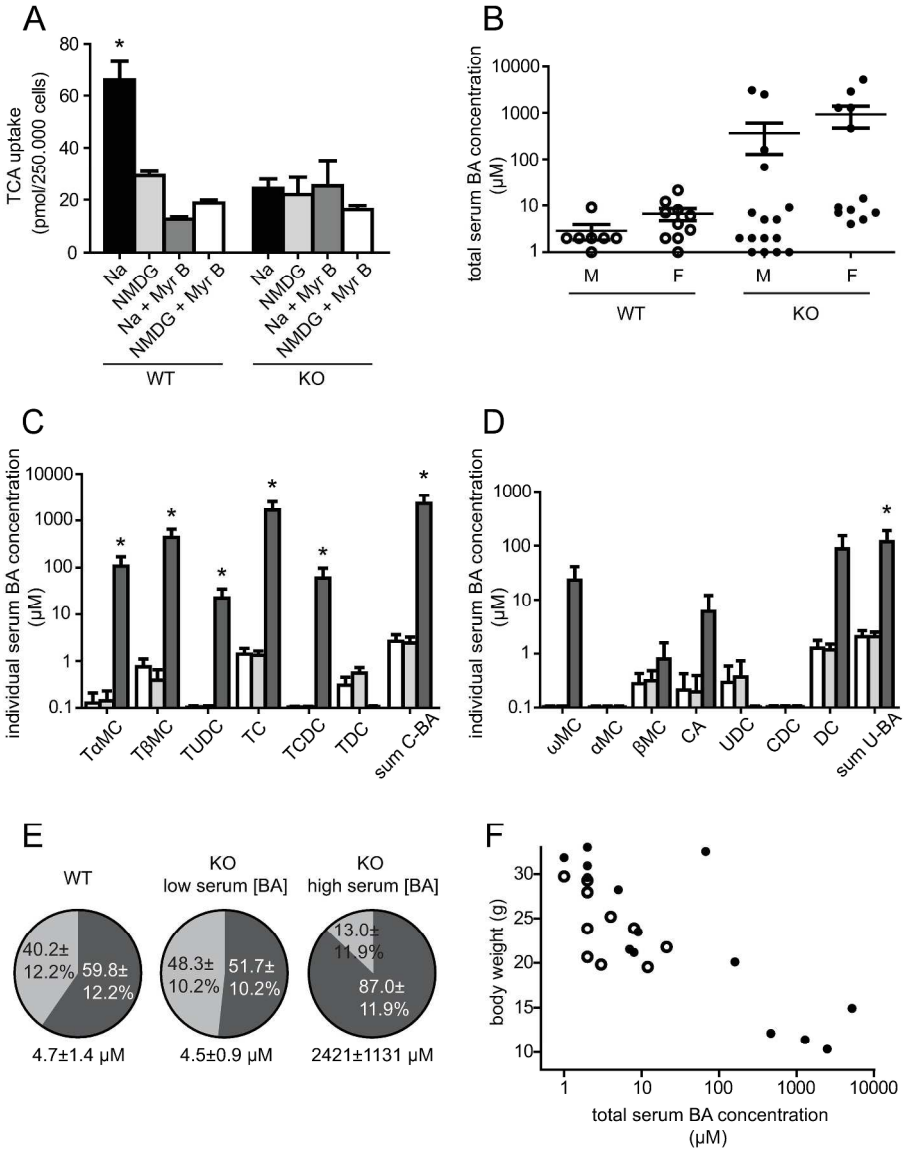

274x364mm (300 x 300 DPI)

Figure 3

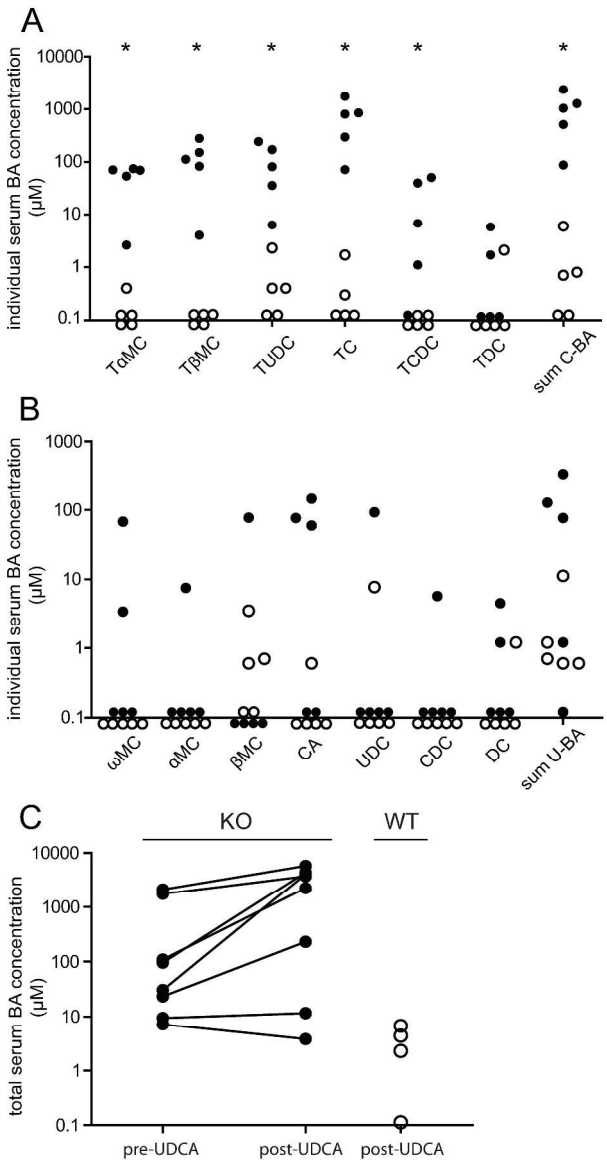

282x470mm (300 x 300 DPI)

Figure 4

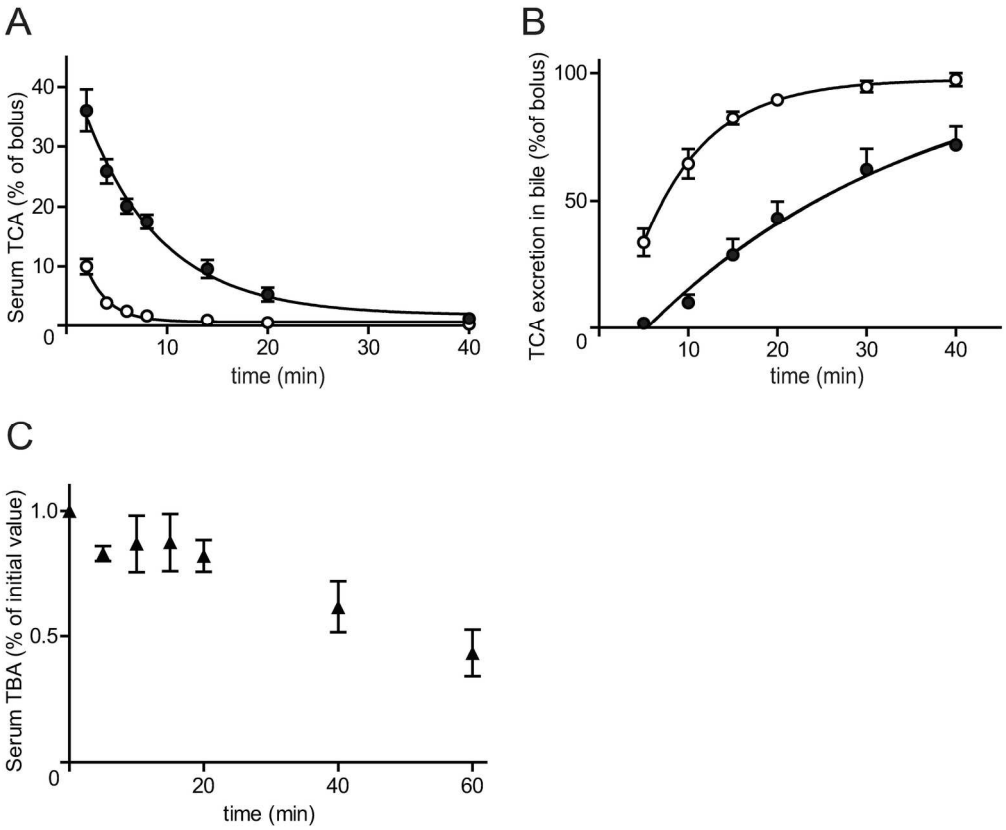

180x164mm (300 x 300 DPI)

Figure 5

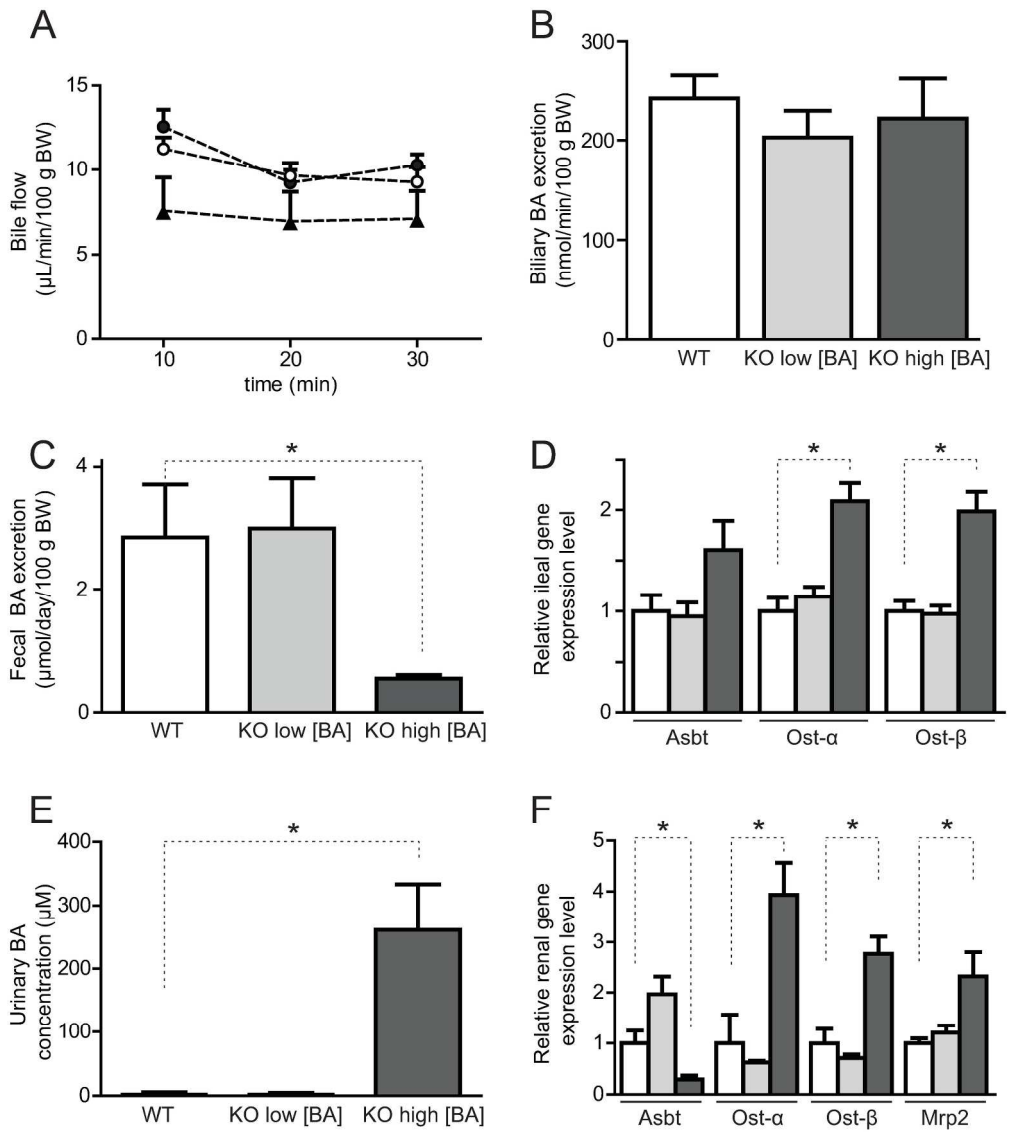

236x279mm (300 x 300 DPI)

Figure 6

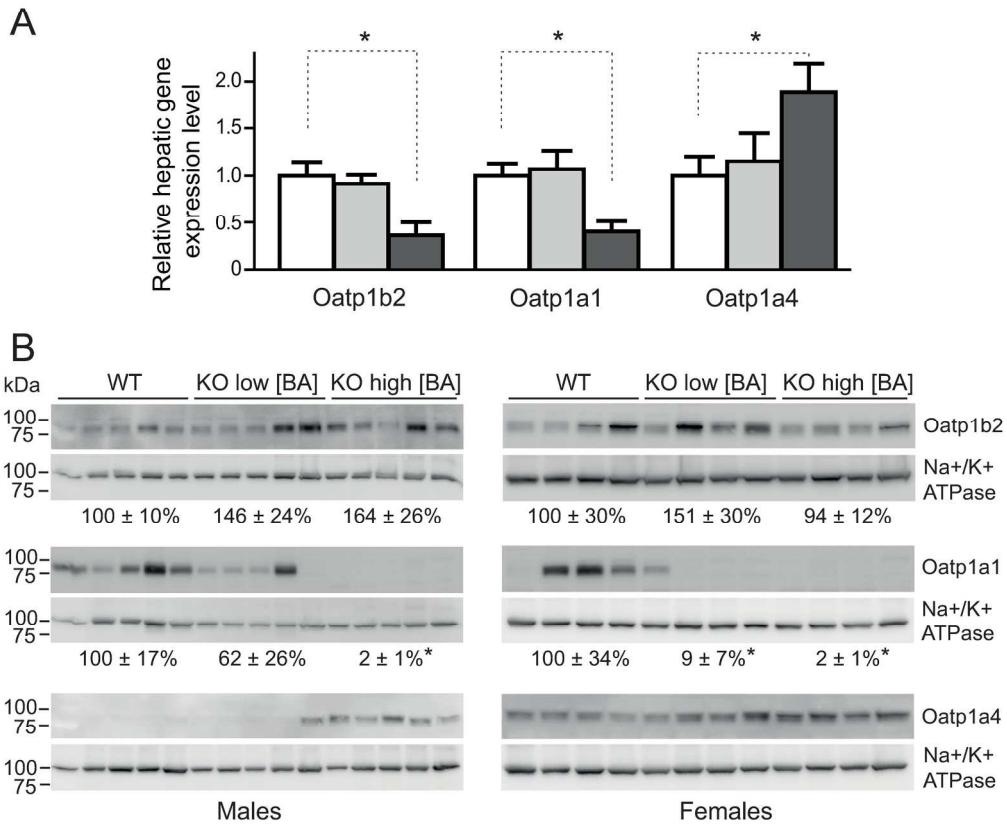

185x170mm (300 x 300 DPI)

Figure 7

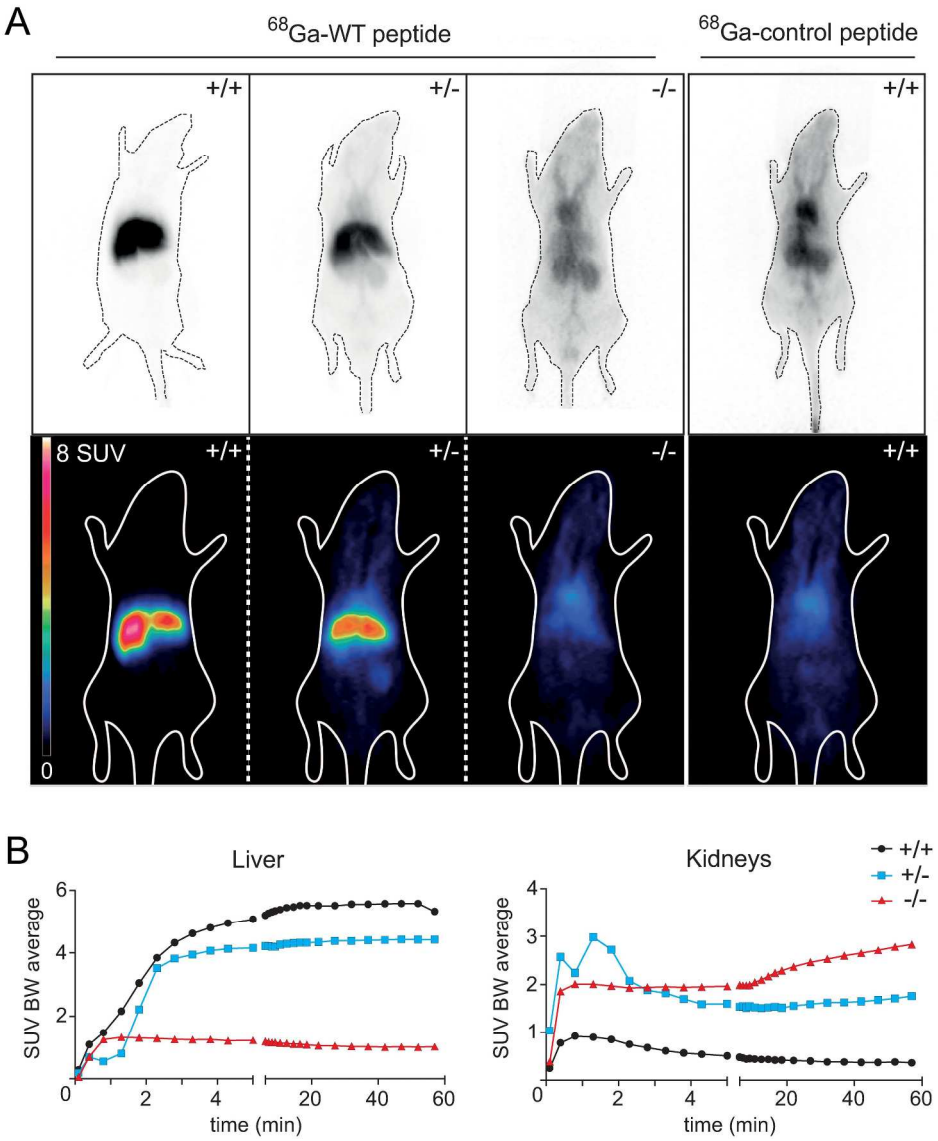

245x301mm (300 x 300 DPI)

Table 1: Body weight development of wild-type (WT) and all *Slc10a1*$^{-/-}$ (KO) mice. Male and female body weights are shown (n=7-17 per group). Values are given as mean ± S.E.M. Asterisk indicates p-value below 0.05.

Body weights	Unit	WT	KO	p-value
Males (2-3 week old)	grams	6.6 ± 0.6	7.0 ± 0.6	0.71
(5-6 week old)	grams	21.0 ± 0.8	13.6 ± 1.6	0.001*
(8-9 week old)	grams	24.6 ± 0.9	19.9 ± 1.4	0.02*
Females (2-3 week old)	grams	7.7 ± 0.6	7.0 ± 0.6	0.41
(5-6 week old)	grams	17.3 ± 0.4	14.7 ± 0.7	0.02*
(8-9 week old)	grams	20.4 ± 0.4	17.8 ± 0.8	0.03*

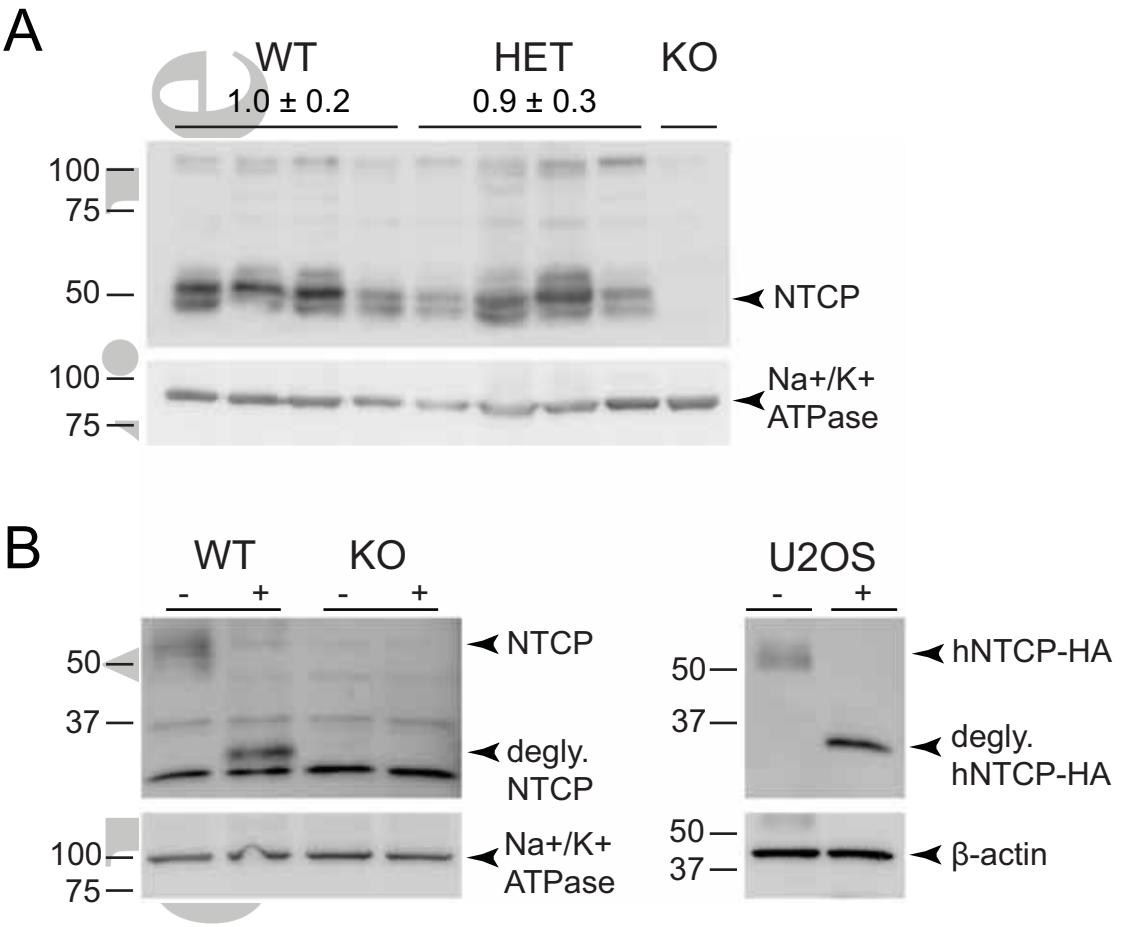

Supplementary Figure 2

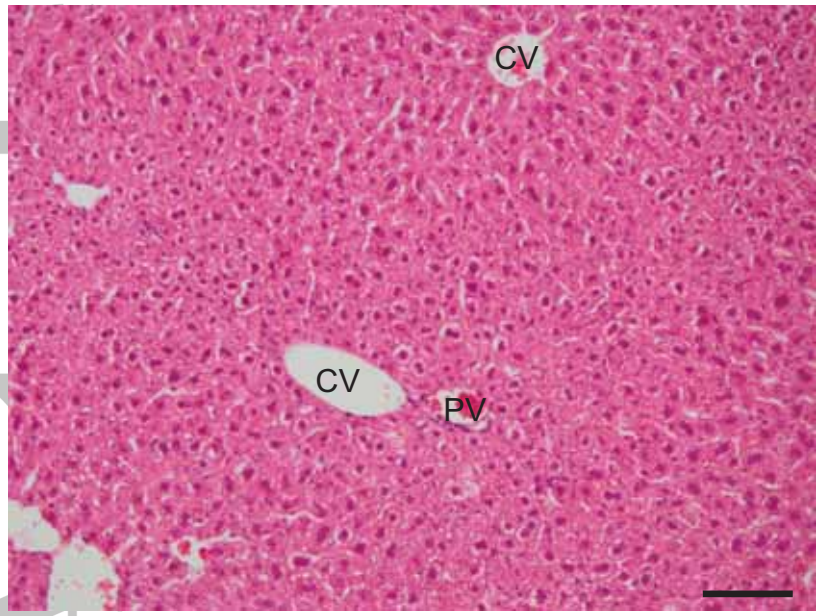

WT

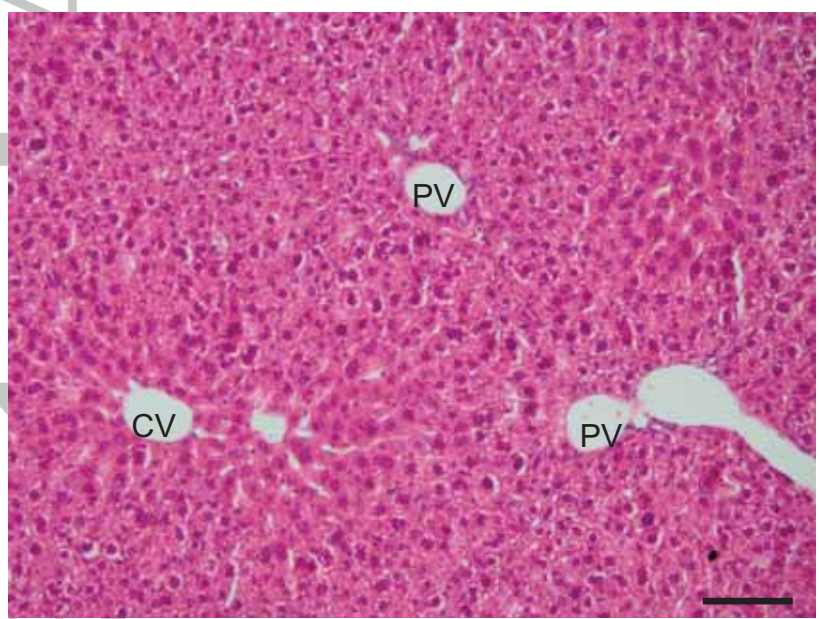

KO low serum [BA]

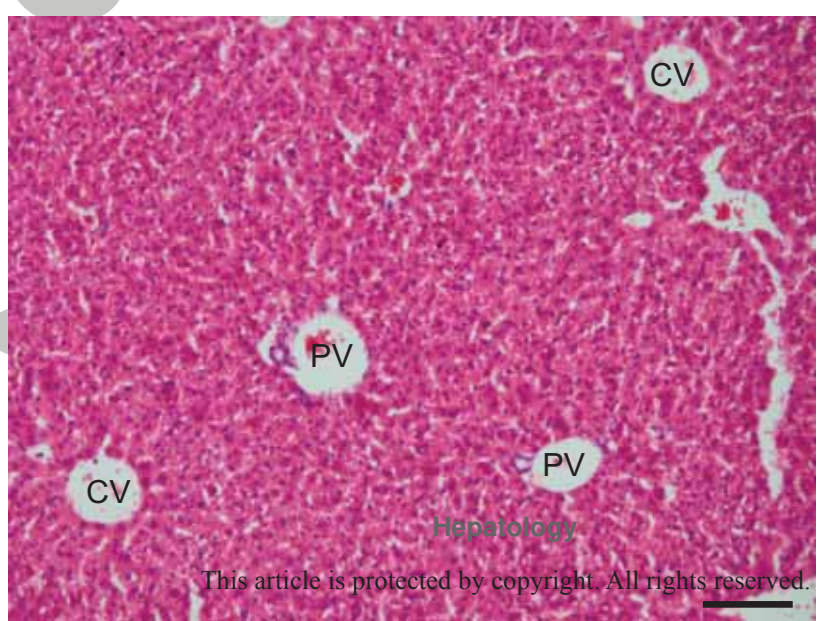

KO high serum [BA]

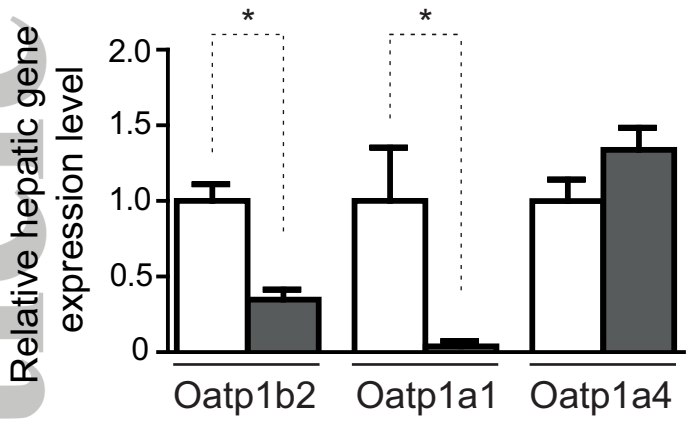

Supplementary Figure 4

A

^{68}Ga-WT peptide (myr-K(^{68}Ga-DOTA)-HBVpreS3-48y)

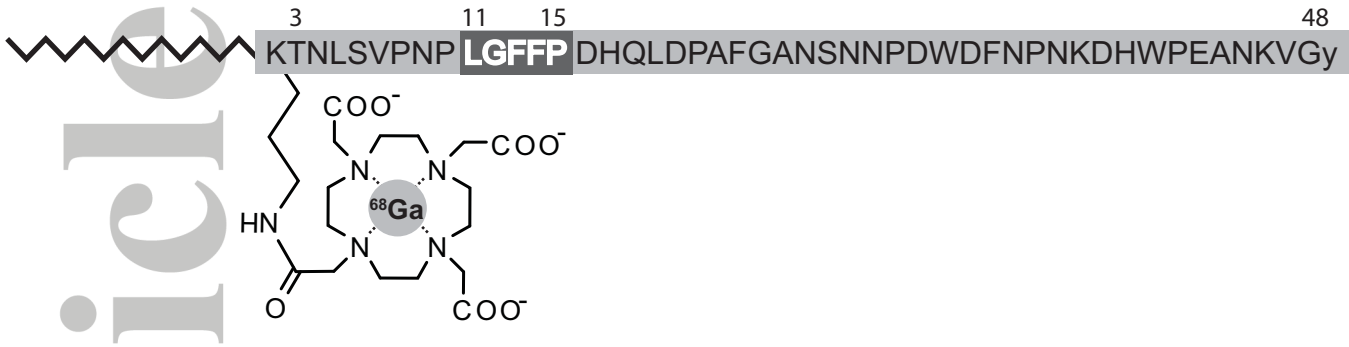

^{68}Ga-control peptide (myr-K(^{68}Ga-DOTA)-HBVpreS3-48y Ala11-15)

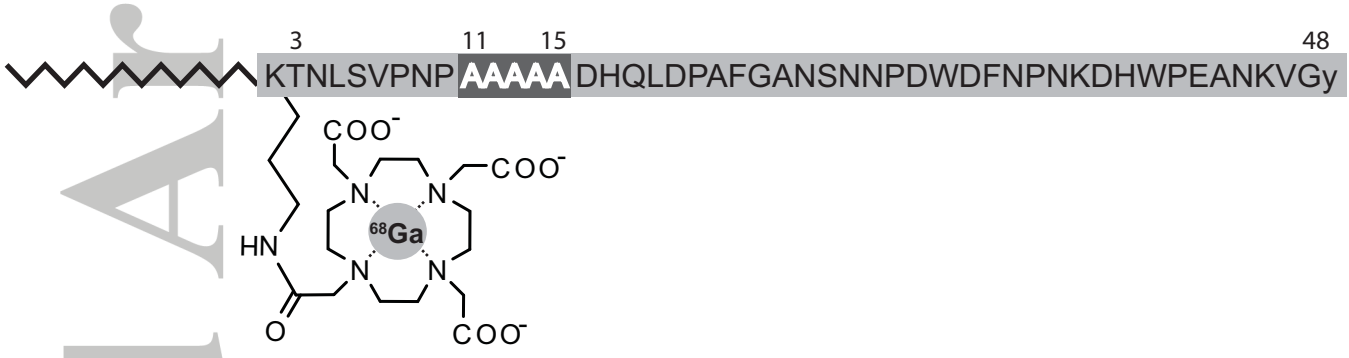

B

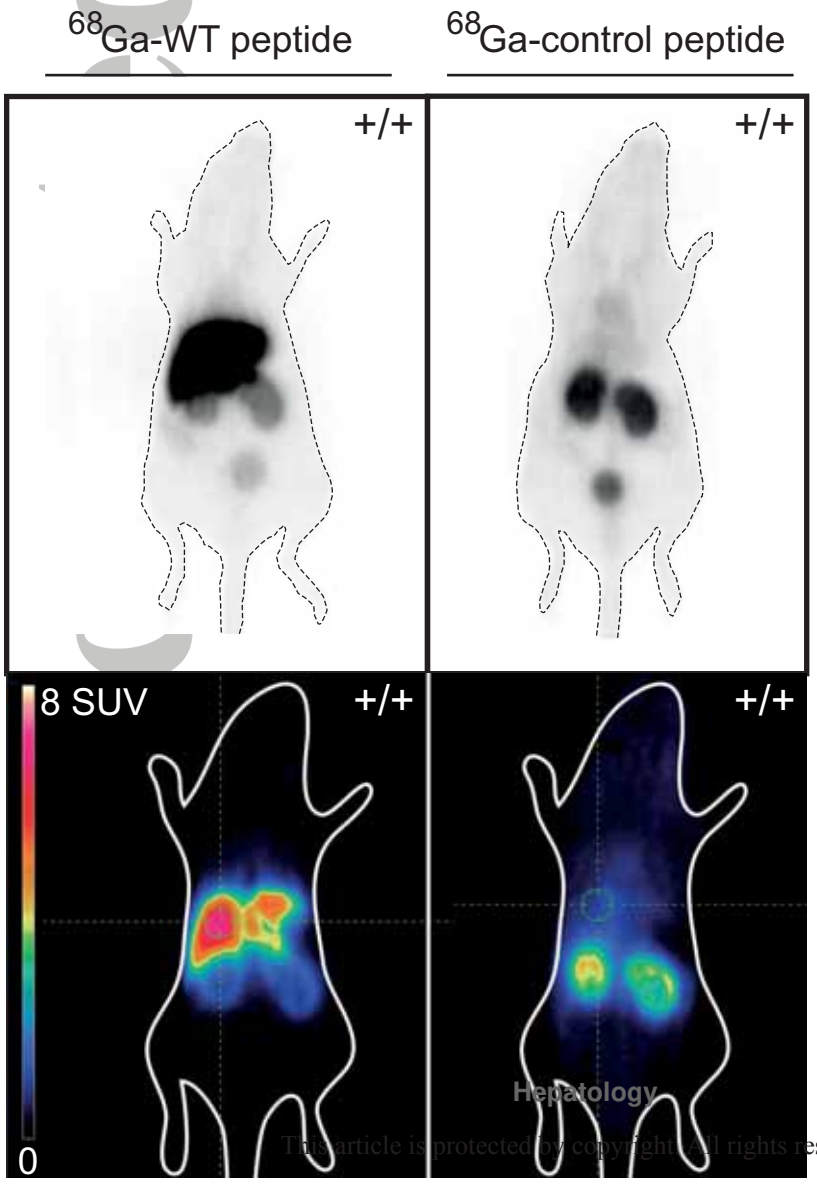

Supplementary materials & methods

Gene-targeting strategy and generation of Slc10a1$^{-/-}$ mice

Mice heterozygously lacking exon 1 of *Slc10a1* were generated by Lexicon Genetics Incorporated (The Woodlands, Texas, US), and obtained via Taconic (Hudson, NY, US). Exon 1 of *Slc10a1* was replaced using a targeting vector consisting of 5' (7.7-kb) and 3' (1.3-kb) sequence homology arms flanking a β-galactosidase/puromycin (βgeo/puro) selection cassette, as shown in figure 1A. Experiments were performed on 6 to 10 week-old *Slc10a1$^{-/-}$* male and female mice using littermate controls, unless stated otherwise. All mice were kept on a 12h light-dark cycle and received a standard chow (SDS, Witham, England) and water *ad libitum*. In one experiment, 0.1% (w/w) ursodeoxycholic acid (UDCA; Sigma-Aldrich) was supplemented to standard chow for 4-8 days. The study design and all protocols for animal care and handling were approved by the Institutional Animal Care and Use Committee of the University of Amsterdam.

RNA isolation and qRT-PCR

Total RNA was isolated from approximately 50 mg of liver, terminal ileum and kidney with TRIzol reagent (Invitrogen, Bleiswijk, The Netherlands). RNA integrity was assessed by agarose gel electrophoresis and spectrophotometrically at 260 nm using a Nanodrop 1000 (Thermo Scientific, Wilmington, US). Five-hundred nanograms of total RNA were treated with DNAse (Promega, Madison, US) and first-strand cDNA was synthesized with Oligo-$dT_{12\text{-}18}$ and Superscript II reverse transcriptase (Invitrogen). Quantitative real-time PCR (qRT-PCR) was carried out in a Roche Lightcycler 480 II instrument using SensiFAST SYBR No-ROX kit (Bioline, UK) and was analysed using LinRegPCR 12.5 software. Expression levels in each sample were normalized for the geometrical mean of two reference genes (supplementary table 2 shows qPCR primer sequences).

Western Blot analysis

Crude mouse liver membranes were isolated by pestle homogenization on ice in hypotonic lysis buffer (10 mM KCl, 1.5 mM $MgCl_2$, 10 mM Tris-HCl pH 7.4) supplemented with protease inhibitor cocktail (Complete, Roche, Mannheim, Germany). Liver homogenates were subjected to ultracentrifugation (200,000 x g, 45 minutes) and the pellets were resuspended in RIPA buffer (50 mM Tris-HCl, pH 8.0, 150 mM NaCl, 1% (v/v) NP-40, 0.5% (w/v) Na-deoxycholate, 0.1% (w/v) SDS). Samples were treated with PNGase F according to the manufacturer's protocol (New England Biolabs), with the exception that denaturation of the samples was performed at 37 °C for 5 min. Membrane proteins (50 µg/lane) were separated on a 10% SDS-polyacrylamide electrophoresis gel, transferred to nitrocellulose and probed with rabbit anti-mouse NTCP or anti-rat OATP1A1 (kind gifts of B. Stieger, Zürich, Switzerland), anti-mouse OATP1A4 (Santa Cruz: sc-18436), or anti-mouse OATP1B2 (kind gift of R. B. Kim, London, Canada) antibodies. As a positive control for NTCP, U2OS cells (human bone osteosarcoma epithelial cells) stably transfected with hNTCP-HA were analysed by Western blot, as previously described (1). Equal loading was ensured by reprobing the membrane with an anti-sodium/potassium ATPase antibody (kind gift of J. Koenderink, Nijmegen, the Netherlands) or with an anti-β-actin antibody (Abcam; ab8226). Immune complexes were detected with a horseradish peroxidase-conjugated secondary antibody (Biorad), visualized using enhanced chemiluminescence detection reagent (Lumi-light, Roche) and detected using ImageQuant LAS 4000 (GE Healthcare). Densitometry was performed in ImageJ software.

Histology and immunohistochemistry

Livers were fixed in 4% PFA overnight, dehydrated in 70% ethanol, and paraffin-embedded. For routine histological tissue examination, hematoxylin-eosin stainings were investigated in wild-type and *Slc10a1*$^{-/-}$ mice. For specific NTCP staining, small cubes of fresh frozen liver tissue were embedded in OCT (Agar Scientific), and 7 µm cryosections were fixed in 100% acetone for 10 minutes. Slides were blocked with 5% (v/v) normal goat serum in PBS +

0.05% (v/v) tween-20 (blocking buffer) for 1 hour, followed by incubation with rabbit anti-mouse NTCP antibody in blocking buffer for 1 hour. After washings, the slides were incubated with goat anti-rabbit Alexa 568 IgG. Images were captured with a Leica SP8X confocal microscope.

Primary hepatocyte isolation and sandwich culture

Primary mouse hepatocytes (PMHs) were isolated from wild-type and *Slc10a1*$^{-/-}$ mice by a 2-step collagenase perfusion method. The liver was perfused through the portal vein with Ca^{2+}-free Krebs/Henseleit-bicarbonate buffer (pH 7.4) saturated with O_2/CO_2 (95:5 v/v) at 37 °C for 10 min, followed by perfusion for an additional 10 min with 20 mg collagenase type IV (0.5 mg/mL) and $CaCl_2$ (1.7 µmol/L). The softened liver was transferred to a sterile plastic dish, and cells were dispersed with a coarse comb in Ca^{2+}-containing Krebs/Henseleit-bicarbonate buffer (pH 7.4), and filtered through nylon gauze. The filtrate was washed and centrifuged three times 3 min at 60 x g, with a final wash in buffer containing 1% (w/v) BSA. Routinely, 30-40 million cells were obtained with viability of at least 85%, as determined by trypan blue exclusion. Next, cells were plated in Dulbecco's modified Eagle's medium (DMEM) supplemented with 2 mM L-glutamine, 100 U/L penicillin/streptomycin and 5% FCS at 250,000 cells per well in 24-wells plates pre-coated with rat-tail collagen type I (1,5 mg/ml, pH 7.4, BD Biosciences). After 3 hours for attachment at 37 °C, a second collagen layer was added to obtain a sandwich configuration, as described by Annaert (2), and cells were cultured another hour in DMEM supplemented with 2 mM L-glutamine and 100 U/L penicillin/streptomycin.

Taurocholic acid uptake assay

After a 30-minute pre-incubation at 37 °C in sodium-containing uptake buffer (136 mM NaCl, 5 mM KCl, 1.1 mM KH_2PO_4, 1 mM $MgCl_2$, 1.8 mM $CaCl_2$, 10 mM D-Glucose, 10 mM HEPES, pH 7.4) with and without Myrcludex B (1 µM), PMHs were incubated at 37 °C for 1 minute with uptake buffer containing 10 µM TCA of which a trace amount (0.1 µM) was

tritium-labelled ([3H]TCA, Perkin Elmer, Groningen, The Netherlands). To assess sodium-dependence of the TCA uptake, NaCl was replaced with equimolar N-methyl-D-glucamine (NMDG). Cells were washed four times with ice-cold PBS buffer and lysed with milliQ water containing 0.05% (w/v) SDS. Radioactivity in the lysates was measured by liquid scintillation counting. Data are presented of two independent PMH isolations, each condition performed in triplicate. All values for TCA uptake were corrected for nonspecific binding by subtracting signal determined in control dishes without cells.

Quantification of bile acids

Feces were collected (24 h) from individually housed mice (to avoid coprophagy), lyophilized and weighed. The dried stools were homogenized and BAs were extracted in 50% (v/v) t-butanol (Merck). Total BA concentrations in feces, urine and serum were quantified with the Total Bile Acid Assay kit (Diazyme Laboratories, Poway, US) by measuring absorbance at 410 nm using a NOVOstar analyzer (BMG-Labtech, Offenburg, Germany). Concentrations of different BA species in serum were determined by reverse-phase HPLC. For HPLC, serum was deproteinized by adding dropwise 5 volumes of acetonitrile (Biosolve, Valkenswaard, The Netherlands), followed by vortex-mixing, centrifugation at 12,000 x g for 10 min and vacuum-drying of the supernatant. Serum BAs were solubilized in 25% methanol. 100 µl was applied to a Hypersil C18 (3 µm, 15 cm HPLC column, Thermo Scientific, Breda, The Netherlands). Starting eluent consisted of 6.8 mM ammonium formate (pH 3.9), followed by several steps of linear gradients to different concentrations of acetonitrile (Biosolve, Valkenswaard, The Netherlands). Detection was performed using a Nano Quantity Analyte Detector QT-500 (Quant technologies, Blaine, US). Quantification of the different BA species was performed using calibration curves for all BA species.

Bile secretion and TCA elimination in vivo

To investigate bile secretion in fasted *Slc10a1*$^{-/-}$ mice, gall bladder cannulation and bile collection was performed. Bile was collected in aliquots every 10 minutes for 30 minutes

after distal ligation of the common bile duct, as described in (3). Bile flow was determined gravimetrically assuming a density of 1 g/mL for bile. Bile output was the calculated as the product of the bile flow and the bile concentration in the second 10-minute collection period. After the 30 minutes depletion-phase, a single bolus of 150 µmol TCA / kg mouse (including a trace amount of tritium-labelled TCA) was administered intravenously in the tail vein in 100 µL 0.9% NaCl per 20 g mouse. A heating pad maintained body temperature at 37 °C. Blood samples (~30 µL) were collected at 30 minutes before TCA administration and both blood and bile were collected at the indicated time points after TCA administration. Radioactivity in serum and bile was measured by liquid scintillation counting, and values are shown as a percentage of the total bolus (=100%). During the gall bladder cannulation experiment without prior TCA administration, blood was collected directly before bile collection.

Peptide synthesis, ^{68}Ga-labelling and PET-imaging

Myrcludex B-derived myristoylated HBV preS1 peptides were synthesized on a solid phase matrix using fluorenylmethoxycarbonyl/*t*-butyl (Fmoc/*t*Bu) chemistry, as previously described (4). For selective coupling of DOTA to the N-terminal lysine side chain on the solid phase, the building block Fmoc-Lys(Aloc)-OH was used. After myristoylation the Aloc orthogonal protecting group was selectively removed and the peptide was reacted with DOTA-DFP, as previously described (5). Following cleavage from the resin, the peptides were purified using preparative high-pressure liquid chromatography (HPLC) and analysed by mass spectrometry (WT-peptide myr-K(DOTA)HBVpreS3-48y; $m/z_{calculated}$: 6015.9283; $m/z_{observed}$: 6016.0201; control-peptide myr-K(DOTA)HBVpreS3-48y Ala11-15; $m/z_{calculated}$: 5809.8188; $m/z_{observed}$: 5809.9182). Peptides are depicted schematically in supplementary figure 4. For ^{68}Ga-labelling, 1000 µl [^{68}Ga]Ga^{3+} eluate, 20 µl of a 1 mM peptide solution in DMSO, 10 µl ascorbic acid solution (20% in H_2O) and 295 µl 2.5 M sodium acetate were mixed (pH 3.6) and heated at 90 °C for 15 minutes. The labelled product was purified using solid phase extraction (Thermo Scientific, Schwerte, Germany). The peptide was eluted from the cartridge with 2 ml ethanol. The ethanol was evaporated, the peptide dissolved in 60 µl

DMSO and 240 µl of 0.9% NaCl were added. The solution was filtered with a 0.22 µM sterile filter prior to injection. Mice were anesthetized with 1% sevoflurane (Abbott, Wiesbaden, Germany) and placed into an Inveon small animal PET scanner (Siemens, Knoxville, US) in a prone position. Investigators were blinded to mouse genotypes. A dynamic microPET was performed up to 60 min post-injection with ^{68}Ga-labelled peptides (6 to 27 MBq/animal in a 100 µl peptide solution in a tail vein). For pretesting of the peptides, female NMRI mice 6 to 8 weeks of age were injected with ^{68}Ga-labelled peptides and static images were taken from 60-80 min post-injection.

Statistical analysis

Data are provided as the mean ± standard error of the mean. Differences between groups were analysed using 2-tailed Student's t-test. For serum and bile kinetics, half-time ($t_{1/2}$) and one-phase decay curves were calculated using Graphpad Prism 5. Statistical significance was considered at $p < 0.05$.

References

1. Bijsmans IT, Bouwmeester RA, Geyer J, Faber KN, van de Graaf SF. Homo- and heterodimeric architecture of the human liver Na^+-dependent taurocholate cotransporting protein NTCP. Biochem J 2012 Feb 1;441(3):1007-15.

2. Annaert PP, Brouwer KL. Assessment of drug interactions in hepatobiliary transport using rhodamine 123 in sandwich-cultured rat hepatocytes. Drug Metab Dispos 2005;33:388-394.

3. Oude Elferink RP, Ottenhoff R, van Wijland M, Smit JJ, Schinkel AH, Groen AK. Regulation of biliary lipid secretion by mdr2 P-glycoprotein in the mouse. J Clin Invest 1995;95:31-38.

4. Schieck A, Müller T, Schulze A, Haberkorn U, Urban S, Mier W. Solid-phase synthesis of the lipopeptide Myr-HBVpreS/2-78, a hepatitis B virus entry inhibitor. Molecules 2010;15:4773-4783.

5. Mier W, Hoffend J, Kramer S, Schuhmacher J, Hull WE, Eisenhut M, Haberkorn U. Conjugation of DOTA using isolated phenolic active esters: the labeling and biodistribution of albumin as blood pool marker. Bioconjug Chem 2005;16:237-240.

Supplementary tables and figures

Supp. table 1: Primer sequences used for amplification of the mouse *Slc10a1* gene by polymerase chain reaction (PCR).

Gene name	Sense and antisense	Product length
Slc10a1 (wild-type allele)	5'-CATCTGACCAGCATTGAGGC-3'	412-bp
	5'-GTTCTGAGGAACTCTTTCATC-3'	
Slc10a1 (targeted allele)	5'-GGTCTCCGAGACTGAGCTAG-3'	624-bp
	5'-CCCTAGGAATGCTCGTCAAGA-3'	

Supp. table 2: Oligonucleotide primers used for qRT-PCR analysis of wild-type and *Slc10a1*$^{-/-}$ (each used at a final concentration of 5 µM). Genes of interest are involved in hepatic sinusoidal BA uptake (*Slc10a1, Slco1a1, Slco1a4, Slco1b2*), intestinal and renal BA transport (*Slc10a2, Slc51a and Abcc2*). Reference genes (*Rplp0, Tbp, Ppib and Hprt*) are also shown.

Gene name	Sense and antisense	Product length	Used in
Slc10a1	5'-TGGCTACCTCCTCCCTGATG-3'	380-bp	Liver
	5'-GCCAGGTTGTGTAGGAGGAT-3'		
Slco1a1	5'-TGAGAAAGACAGCAGTAGGACTTT-3'	162-bp	Liver
	5'-GTGATTTGGCTAGGTATGCAC-3'		
Slco1a4	5'-TACATGTCAGCTTGCCTCGC-3'	140-bp	Liver
	5'-GCACACTCAGGACCCTTGTC-3'		
Slco1b2	5'-GGGTGAATGCCCAAGAGACA-3'	282-bp	Liver
	5'-TATAGCCTGCATGCTCCACG-3'		
Slc10a2	5'-CCATGGGGTATCTTCGTGGG-3'	278-bp	Ileum, kidney
	5'-GTTCCCGAGTCAACCCACAT-3'		
Slc51a	5'-GGCATCTATGACCCAGGAGA-3'	151-bp	Ileum, kidney
	5'-TGGATCCCATGTTCTGTTCA-3'		
Slc51b	5'-GACCACAGTGCAGAGAAAGC-3'	102-bp	Liver
	5'-ATTCCAAGGAGCCGCATCT-3'		
Abcc2	5'-AGCAGGTGTTCGTTGTGTGT-3'	133-bp	Kidney
	5'-AGCCAAGTGCATAGGTAGAGAAT-3'		
Rplp0	5'-CCAGCGAGGCCACACTGCTG-3'	169-bp	Liver, kidney
	5'-ACACTGGCCACGTTGCGGAC-3'		
Tbp	5'-GGAGAATCATGGACCAGAACA-3'	89-bp	Liver
	5'-GATGGGAATTCCAGGAGTCA-3'		

Ppib	5'-TCGGAGCGCAATATGAAGGT-3'	65-bp	Ileum
	5'-AAAAGGAAGACGACGGAGCC-3'		
Hprt	5'-TTGCTCGAGATGTCATGAAGGA-3'	91-bp	Ileum
	5'-AGCAGGTCAGCAAAGAACTTATAG-3'		

Supp. table 3: Liver weights and biochemical indicators in serum of 2-month-old wild-type, normocholanemic and hypercholanemic *Slc10a1*$^{-/-}$ mice. Female mice were included (n=4-5 per group). AST: aspartate aminotransferase. ALT: alanine aminotransferase. ALP: alkaline phosphatase. Values are given as mean ± S.E.M. Asterisk indicates p-value below 0.05.

Parameter	Unit	wild-type	KO low BA	KO high BA
Liver weight	% of body weight	5.2 ± 0.2	5.0 ± 0.2	5.2 ± 0.2
Serum total bilirubin	µmol/L	3.2 ± 0.7	7.2 ± 3.4	24.8 ± 7.5 *
Serum conjugated bilirubin	µmol/L	2.6 ± 0.6	8.2 ± 5.8	31.4 ± 8.0 *
Serum AST	U/L	142.5 ± 33.1	186.7 ± 43.6	896.4 ± 403.3
Serum ALT	U/L	58.0 ± 12.5	51.0 ± 15.8	152.8 ± 47.6
Serum ALP	U/L	22.0 ± 6.2	15.9 ± 4.6	219.1 ± 38.8 *

Supp. figure 1: (A) NTCP protein (~45-50 kDa) levels in liver membranes of wild-type (WT) and heterozygous (HET) *Slc10a1* mice. Values are given as mean ± S.E.M., quantified relative to sodium/potassium ATPase (~ 90 kDa) and normalized to wild-type levels (set at 1.0). Liver membrane homogenate of one *Slc10a1*$^{-/-}$ (KO) mouse was included as negative control. (B) Mouse NTCP protein size without (-) and with (+) *N*-glycosidase PNGase F treatment (left panel). As a positive control, deglycosylation of HA-tagged hNTCP, stably transfected in U2OS cells, was shown by Western blot analysis (right panel). β-actin served as a loading control.

Supp. figure 2: Liver hematoxylin-eosin histology comparing adult male wild-type and *Slc10a1*$^{-/-}$ mice. Both knockout mice with normal serum BAs and high serum BAs were investigated. Section thickness is 7 µm. Portal vein (pv) and central vein (cv) are indicated. Scale bar is 100 µm.

Supp. figure 3: Relative mRNA expression levels of the *Oatp*-isoforms were calculated for wild-type and hypercholanemic *Slc10a1*$^{-/-}$ mice upon dietary supplementation with 0.1% UDCA. Values are given as mean ± S.E.M. for 4-6 adult female mice per group. Asterisk indicates p-value below 0.05.

Supp. figure 4: (A) Schematic representation of ^{68}Ga-WT peptide (top) and ^{68}Ga-control peptide (bottom). (B) microPET-based pretesting of the Myrcludex-B-derived peptides in female wild-type NMRI mice. Top: Uncorrected planar projection, bottom: coronal PET section.